Master thesis

Modelling of Microstructure in TRIP-Assisted steels

Guo, Lei (郭磊)

Department of Ferrous Technology

Graduate Institute of Ferrous Technology

Pohang University of Science and Technology

2007

Modelling of Microstructure in TRIP-Assisted steels

Modelling of Microstructure in TRIP-Assisted steels

By

Guo, Lei

Department of Ferrous Technology

(Computational Metallurgy)

Graduate Institute of Ferrous Technology

Pohang University of Science and Technology

A thesis submitted to the faculty of Pohang University of Science and Technology in partial fulfillments of the requirements for the degree of Master of Science in the Graduate Institute of Ferrous Technology (Computational Metallurgy)

Pohang, Korea
28 June, 2007

Approved by

Prof. Liu, Weijie _____

Prof. Bhadeshia, H.K.D.H. _____

Major Advisor

Modelling of Microstructure in TRIP-Assisted steels

Guo, Lei

This dissertation is submitted for the degree of Master of Science at the Graduate Institute of Ferrous Technology of Pohang University of Science and Technology. The research reported herein was approved by the committee of Thesis Appraisal

28 June, 2007

Thesis Review Committee

Chairman: Qin, Rongshan _____

Member: Kim, Kyoo Young _____

Member: Kim, In Gee _____

MIS Guo, Lei

20052852 Modelling of Microstructure in TRIP-Assisted steels

Adivisor: Liu, Weijie; Bhadeshia, H.K.D.H.
Text in English

Abstract

A carbon diffusion-controlled intercritical annealing model has been developed. Calculations show that paraequilibrium will not be reached in typical intercritical annealing process times of around 3 minutes. The pearlite colony size has a big influence on the kinetics of austenitisation in intercritical annealing. Fine pearlite can accelerate austenite formation.

Paraequilibrium thermodynamic calculations show that the substitution of Si by P has little effect on Ae_1' and Ae_3' transformation temperatures. Replacement of Si by Al, however, shifts these temperatures to appreciably higher values and effectively eliminates the presence of a fully austenitic region.

A carbon-diffusion controlled bainite transformation model has also been developed. The results show that Al can retard the diffusion of carbon during the bainite transformation. Si and P also have the same effect, but to a smaller extent.

A theoretical framework for modelling the effect of Si additions on cementite nucleation kinetics has been developed. Si retards the cementite nucleation rate by a factor of:

$$R_J = \exp\{-(G^*/kT)[1/(1-x_{Si}\Delta g_b/\Delta g_{\gamma/cm})^2 - 1]\}$$

Back-calculation was used to determine the energy difference induced by Si addition.

The model shows that a higher bainite transform temperature leads to more rapid cementite precipitation in low-Si steel.

Contents

Abstract I

Contents III

Nomenclature V

Introduction 1

I TRIP-assisted steels 3

1.1 Microstructure evolution 7

1.2 Cold-rolled TRIP-assisted steel 8

1.2.1 intercritical annealing 9

1.2.2 Isothermal transform to bainite 10

1.3 Alloying elements in TRIP-assisted steel 11

1.4 Summary 14

II Modeling of intercritical annealing 16

2.1 Construction of Model 17

2.2 Results and discussion 23

2.2.1 Thermodynamic Calculations 23

2.2.2 Kinetic Calculations 28

2.2.2.1 Influence of chemical composition 31

2.2.2.2 Influence of the starting microstructure 33

2.2.2.3 Influence of intercritical annealing temperature 35

2.3 Summary 38

III Modeling of isothermal bainite transformation 40

3.1 Construction of Bainite Transformation Model 41
3.2 Construction of Cementite Precipitation Model 47
3.3 Combination of the bainite plate growth and cementite precipitation model 53
3.4 Results and Disscusion 55
3.4.1 Influence of chemical composition 57
3.4.2 Influence of bainitic transformation temperature 62
3.4.3 Influence of intercritical annealing temperature 65
3.5 Summary 69
IV Conclusions and Future Work 70
V References 72
Acknowledgements 79

Nomenclature

Term	Meaning
α	Allotriomorphic ferrite
α_b	Bainitic ferrite
α'	Martensite
$\alpha 1$	One-dimensional parabolic rate constant for diffusion-controlled growth
$\alpha 3$	Three-dimensional parabolic rate constant for diffusion-controlled growth
γ	Austenite
θ	Cementite
γ_R	Retained austenite
λ	Bainite interplate spacing
η	Shape factor of the embryo
δ	Energy of austenite/cementite interface per area
A	Attempt frequency
$Ae_1^{'}$	The temperature at which austenite begins to form in paraequilibrium.
$Ae_3^{'}$	The temperature at which transformation of ferrite into austenite is completed in paraequilibrium, in hypoeutectoid steel.

D	Carbon diffusivity in austenite
$\overline{D}$	Average carbon diffusivity over carbon concentration profile
f	Dimensionless supersaturation
$g_{r0.25}$	Free energy per atom of austenite with 0.25 mole fraction of carbon
$g_{\gamma x0}$	Free energy per atom of austenite with the carbon concentration x_0
g_{cm}	Gibbs free energy of cementite per atom
$\Delta g_{\gamma/cm}$	Driving force of transformation from austenite to cementite per iron atom
$\Delta g'_{\gamma/cm}$	Driving force for forming a Si-modified cementite nucleus per iron atom
Δg_b	Energy difference due to introduction of Si of cementite
G^*	Critical energy for cementite nucleation
G'^*	Critical energy for the Si-modified cementite nucleation
I	Nucleation rate
J	Flux
k	Boltzmann constant
L	length of diffusion field
N_0	Number density of nucleation sites
P	Total carbon consumed by cementite precipitation in mole fraction
Q_C	Activation energy for transforming atom from the matrix to

	cementite
r	Radius of pearlite particles
R	Paraequilibrium radius of austenite in intercritical annealing
R_d	Dilution rate of carbon concentration in austenite
t	Time
T	Temperature
v_d	Velocity of austenite/ferrite interface
V_{cm}	Fraction of cementite formed at time t over the equilibrium volume
V_p	Volume fraction of pearlite
V_γ	Volume fraction of austenite
$V_\gamma^{'}$	Paraequilibrium volume fraction of austenite
$x^{\gamma\alpha}$	Carbon mole fraction of austenite in paraequilibrium with austenite
$x^{\alpha\gamma}$	Carbon mole fraction of ferrite in paraequilibrium with ferrite
x'	Far field Carbon mole fraction in austenite following soft impingement
x_{Si}	Mole fraction of Si
x_0	Average austenite carbon mole fraction
z	Position of the moving interface of austenite/ferrite

Introduction

In the recent decades, there has been much interest in lightweight and high strength materials for the automobile industry. To meet the demand, a variety of steels which present a good combination of strength and ductility have been developed. One example is the transformation-induced plasticity (TRIP) steels, which rely on the martensite transformation during deformation.

There are two types of such steels：TRIP steels and TRIP-assisted steels. The former have a fully austenitic microstructure [1], obtained by alloying with a large amount of nickel or other expensive austenite-stabilising elements, making it expensive. TRIP-assisted steel has a complex multiphase microstructure, in which austenite is an important but minor phase [2, 3]. The remainder of the microstructure consists of allotriomorphic and bainitic ferrite. The TRIP-assisted steels are lean in alloying elements, which makes them affordable, with a typical composition Fe-0.2C-1.5Mn-1.5Si wt%. The silicon retards the precipitation of cementite from austenite, which is enriched in carbon due to partitioning from bainitic ferrite. This carbon enrichment allows it to be retained to ambient temperature.

Objective of the present work

As the retained austenite is the key feature in TRIP-assisted steel, it is the aim to develop a model to predict its volume fraction and composition as a function of the average composition of the steel and any heat treatment parameters. There are two production processes, one for completely austenitised hot-rolled sheet subsequently transformed into the appropriate microstructure, and the second beginning with cold-rolled sheet which is intercritically annealed and then transformed. It is the latter on which this work focuses.

An attempt is also made to model the effect of silicon on cementite precipitation kinetics.

Ⅰ TRIP-assisted steels

These alloys have a good balance of strength and ductility, with a microstructure of allotriomorphic ferrite obtained by intercritical annealing, bainitic ferrite, martensite and retained austenite. The latter is responsible for the TRIP effect, *i.e.* a mechanically-induced martensitic transformation.

Typical mechanical properties of automotive steels such as the 0.2 proof strength (PS), ultimate tensile strength (UTS), total uniform elongation (TEL) and strain-hardening exponent (n) of various automobile steels are listed in Table 1.1. As can be seen in Figure 1.1, any increase in strength is in general associated with a loss of ductility. The exception is the TRIP-assisted steel, where considerable ductility is obtained in spite of the strength, due to transformation-induced plasticity [4].

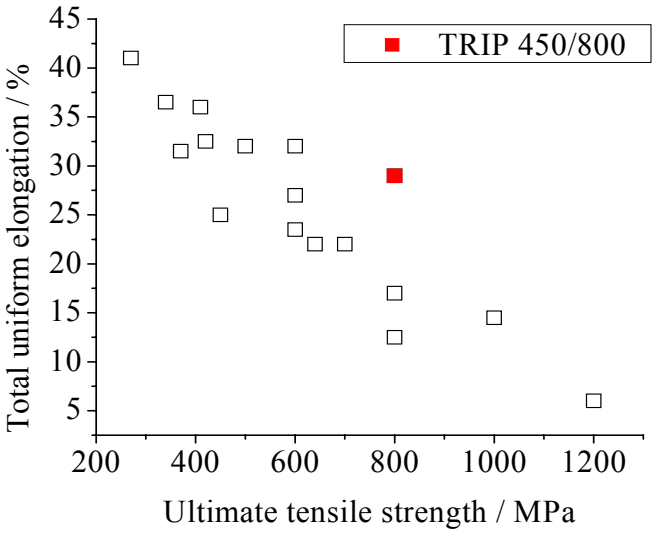

Figure 1.1: Ultimate tensile strength versus total uniform elongation (total uniform elongation is the mean value in table 1.1).

Steel type	PS / MPa	UTS / MPa	TEL / %	n
Mild 140/270	140	270	38-44	0.05-0.15
BH 210/340	210	340	34-39	0.23
BH 260/370	260	370	29-34	0.18
IF 260/410	260	410	34-38	0.13
DP 280/600	280	600	30-34	0.2
IF 300/420	300	420	29-36	0.21
DP 300/500	300	500	30-34	0.2
HSLA 350/450	350	450	23-27	0.16
DP 350/600	350	600	24-30	0.22
DP 400/700	400	700	19-25	0.14
TRIP 450/800	450	800	26-32	0.14
HSLA 490/600	490	600	21-26	0.24
DP 500/800	500	800	14-20	0.13
SF 570/640	570	640	20-24	0.14
CP 700/800	700	800	10-15	0.08
DP 700/1000	700	1000	12-17	0.13
Mart 950/1200	950	1200	5-7	0.09

Table 1.1: Typical mechanical properties of steels for automotive applications [5]. Mild: mild steel or plain carbon steel; BH: bake hardenable steel; IF: interstitial free steel; DP: dual phase steel; HSLA: high strength low alloy steel; TRIP: transformation induced plasticity steel; SF: stretch flanging steel; CP: complex phase steel; Mart: martensitic steel;

In the 1980's, the TRIP effect was demonstrated in low-alloy steels made with 0.2 C, 1-2 Mn and 1-2 Si (wt%) [3]. The microstructures consisted of 50-60 vol.% allotriomorphic ferrite (α), 20-30 vol.% carbide-free bainitic ferrite (α_b), the remainder being high-carbon retained austenite (γ_R) with some martensite (α'), Figure 1.2 [6].

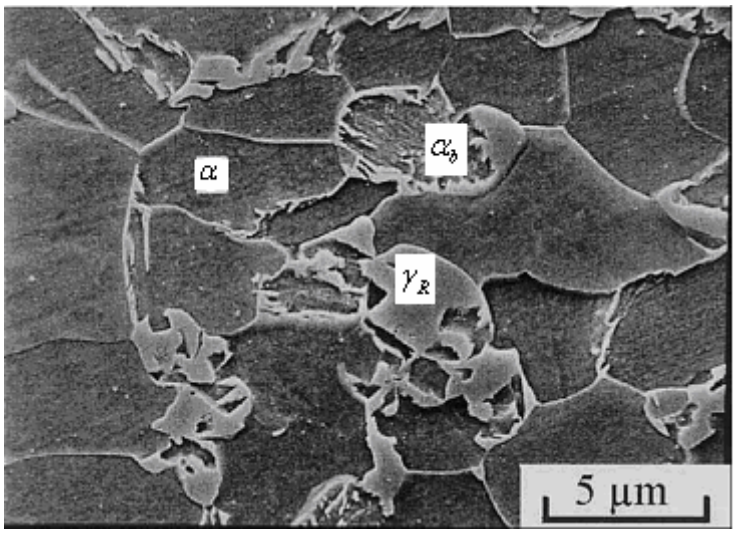

Figure 1.2: Typical multiphase microstructure of a modern TRIP-assistedsteel, with allotriomorphic ferrite (α), carbide-free bainite (α_b) and retained austenite (γ_R) [6].

The major factor influencing the mechanical behaviour of low-alloy TRIP-assisted steels is the stability of the γ_R dispersion, which in turn is affected by chemical composition, particle size and stress-state. These parameters are usually coupled, thus making the optimization of the microstructure and properties a complex task. Hence the need for a model.

C	Si	Mn	Al	P	Nb	Mo	Cu
0.38	1.53	0.83		0.007			
0.18	2.0	1.5	0.037	0.015			
0.19	2.48	1.49	0.036	0.014			
0.11	0.59	1.55	1.5	0.012			
0.14	0.53	1.57		0.204			
0.22	1.55	1.55	0.028		0.035		
0.20	1.47	1.51	0.028	0.004	0.047	0.2	
0.20	1.6	1.6	0.028		0.041	0.3	
0.21	1.49	1.49	0.028	0.005	0.017	0.1	
0.14	1.49	1.51	0.04	0.0012			0.51

Table 1.2 : Typical chemical compositions (wt%) of TRIP-assisted steels [3, 6-11].

To promote austenite it is necessary to suppress cementite precipitation during the bainite reaction. TRIP-assisted steels are therefore alloyed with silicon (1-2.5 wt %) [6] because this solute inhibits cementite precipitation from austenite [6]. However, silicon also affects the surface quality, so other solutes such as aluminium may also be used with identical effects with respect to cementite precipitation [6].

1.1 Microstructure evolution

The required microstructure can be generated using either hot or cold rolled steels. The former involves transformation from a fully austenitic state, followed by cooling to ambient temperature at a rate controlled to allow the

austenite to partially transform into allotriomorphic ferrite and then into bainitic ferrite. In contrast, a two stage annealing treatment is required to produce the desired microstructure beginning with cold-rolled samples (Figure 1.3). The material is heated into the $\alpha+\gamma$ phase field to generate a mixture of ferrite and austenite, the latter subsequently decomposing into bainitic ferrite at a lower temperature.

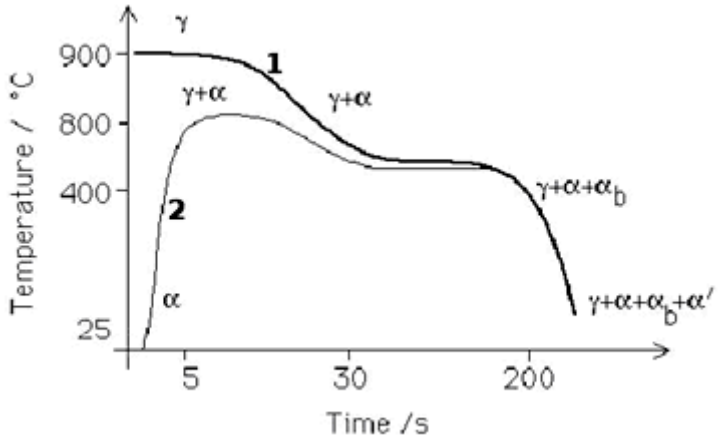

Figure 1.3: Schematic illustration of the two routes to generate the microstructure of TRIP-assisted steel, with typical temperature and time indicated. Curve 1 stands for the transformation from fully austenitic state after hot rolling; curve 2 represents intercritical annealing after cold rolling. The terms γ, α, α_b and α' represent austenite, allotriomorphic ferrite, bainitic ferrite and martensite respectively [12].

1.2 Cold-rolled TRIP-assisted steel

The cold-rolled route generally leads to a better surface quality. The heat

treatment of cold rolled TRIP-assisted steel consists of intercritical annealing and isothermal bainitic soaking. The stabilisation of austenite at room temperature is due to its carbon enrichment all along the thermal scheme. Firstly, carbon concentrates within austenite during the intercritical annealing. Secondly, the bainite transformation is accompanied by carbon redistribution from bainitic ferrite to the surrounding residual austenite.

The amount of retained austenite can increase with average carbon content as shown in Figure 1.4. In cold-rolled and intercritically annealed material, the austenite will nucleate at ferrite/cementite boundaries with dissolution of the cementite, resulting in carbon enrichment in austenite.

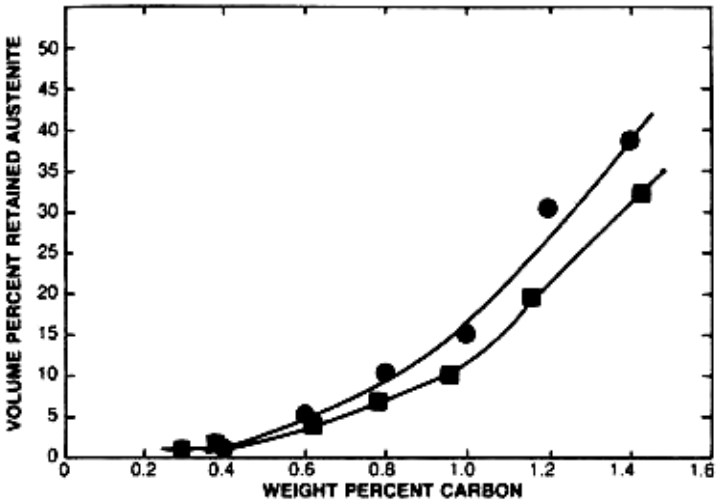

Figure 1.4: Variation of retained austenite with carbon content [13].

1.2.1 intercritical annealing

The starting microstructure of cold-rolled steels consists of allotriomorphic

ferrite and pearlite [14]. It is well established that the austenite forms during heating of ferrite/pearlite microstructures proceeds in two steps [14]. The first step involves the rapid formation of high-carbon γ and dissolution of pearlite. The second step is slower as γ grows and consumes allotriomorphic ferrite.

It is reported that thermodynamic and kinetic calculations set upper and lower limits for carbon concentration and austenite volume fraction in intercritical annealing [14].

1.2.2 Isothermal transform to bainite

Bainite growth is in one hypothesis followed by the rejection of C into austenite shown in Figure 1.5, thus increasing the stability of the final γ_R dispersion. Measurements of carbon-content within individual γ_R particles in various TRIP-assisted steels, have shown considerable C enrichment of γ_R, with concentrations reaching as high as l.25-1.40 wt % C [15].

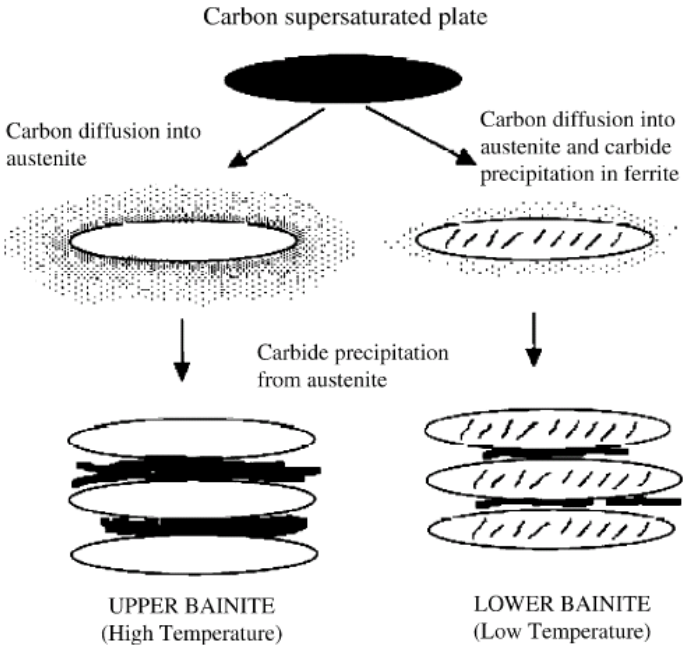

Figure 1.5: An illustration of the growth of bainite and the development of upper and lower bainite [16]

1.3 Alloying elements in TRIP-assisted steel

Alloying elements are added to TRIP steel for the following reasons:

- to optimise the fraction of retained austenite,
- to control cementite precipitation,
- to increase the hardness of ferrite and
- to increase hardenability so that pearlite formation can be avoided.

Manganese

Manganese is an austenite stabilizing element. Significant concentrations

are used in the range 1.5-2.5 wt% to depress the two-phase field, and thus the intercritical temperatures [17]. Manganese increases the solubility of carbon in austenite in equilibrium with cementite, allowing for further enrichment, However, excessive concentrations can promote carbide precipitation in austenite [18]. Manganese, especially in conjunction with silicon, can affect the steel's surface chemistry and make hot-dip galvanising impossible [19].

Silicon

Silicon is usually added to TRIP steels in the range 1.5-2.5 wt% [17] , to allow the retention of austenite [20]. Figure 1.6 shows curves of volume fraction of retained austenite for materials containing two different levels of silicon.

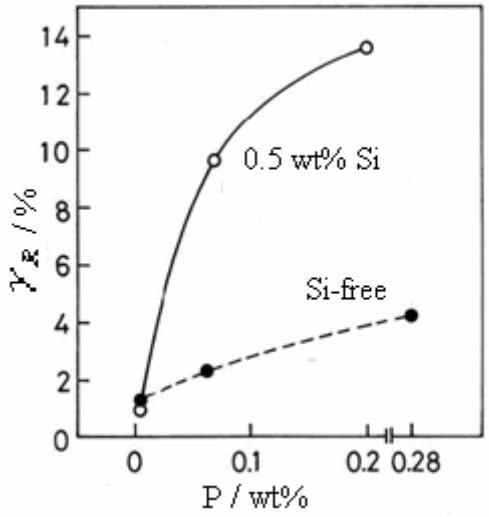

Figure 1.6 Effects of silicon and phosphorus on retained austenite content [21].

Silicon has a very low solubility in cementite [22], and hence retard the precipitation of cementite. This leaves more carbon available for the enrichment and consequential stabilization of the austenite. It has some detrimental effects on galvanisation, due to its segregation to the surface leading to formation of complex manganese-silicon-oxides that resist wetting by zinc [19, 23].

Phosphorus

An increase in phosphorus content enhances the volume fraction of retained austenite, especially in the presence of silicon (Figure 1.8) [21]. Phosphorus also inhibits the formation of cementite, leaving more carbon in solution for segregation to austenite.

Although phosphorus causes cold work embrittlement in low and ultra-low carbon steels, this is not expected to be an issue in TRIP-type steels, as the carbon content is usually in excess of 0.1 wt% [23, 24].

Aluminum

Aluminum decreases also the rate of cementite precipitation[18, 25]. There have recently been attempts to wholly or partially substitute for silicon [24]. Aluminum does not segregate to the surface as silicon does, making Al-containing alloys suitable for galvanising [19, 26], it has been demonstrated that the partial substitution of Si by Al can result in good mechanical properties with an improved formability compared to the conventional C-Mn-Si TRIP-assisted steel [24].

Niobium

Niobium is observed to increase the volume fraction of retained austenite; it is a powerful solid solution hardener, and may result in the mechanical stabilization of the small austenite particles [11, 27, 28]. However, niobium is preferred to form Nb(C,N) which can act as nucleation sites that will accelerate pearlite, thus reducing the carbon available for partitioning into the austenite [27].

Molybdenum

Molybdenum thermodynamically favours the formation of cementite, but its precipitation is very slow because the precipitation process requires the diffusion of Mo [18]. Molybdenum enhances hardenability and it suppresses the formation of pearlite [23].

Copper

Copper delays also the precipitation of cementite [29, 30]. It is also a potent solid-solution and precipitation strengthener, and promotes corrosion resistance [31]. It also stabilises austenite.

1.4 Summary

TRIP-assisted steels present a good combination of strength and ductility, these good properties are rely on the transformation induced ductility, which

is obtained by addition of silicon or aluminium to inhibiting the precipitation of cementite during bainite formation and hence allows carbon to remain dissolved in the untransformed austenite. But the mechanism of the retardation is not fully understood till now.

The microstructure of this steel is complex, making the optimisation of the steel difficult, and hence need for model.

II Modeling of intercritical annealing

There is a lot of work done on cold-rolled TRIP-assisted steel, but the intercritical annealing component of the heat-treatment has received much less attention than the subsequent production of bainite by isothermal transformation [32]. It is important to consider phase transformations which occur upon heating, because the microstructural state after intercritical annealing, *i.e.* volume fraction, chemical composition and homogeneity of austenite, has a great influence on the kinetics of bainite transformation, and hence on the stability of any austenite which is then retained.

It is established that the formation of austenite during the heating of mixtures of ferrite and pearlite occurs in two distinct steps [14]. The first is rapid and involves the formation of austenite from pearlite; in the second slower step, austenite grows to consume allotriomorphic ferrite. These are the issues which form the basis of this Chapter.

2.1 Construction of the Model

The following assumptions are made in creating a mathematical framework for intercritical annealing:

1. The pearlite colonies in the initial microstructure are assumed to have a spherical morphology in three dimensions. The colonies are further assumed to be randomly dispersed in the initial microstructure. It is considered that the transformation of pearlite to austenite occurs so rapidly that it can be assumed to be instantaneous at the intercritical annealing temperature.
2. The conditions once pearlite has been consumed form the basis of the calculations for the second stage of austenite formation.

Consequently, the system is considered initially to consist of high-carbon austenite (replacing pearlite) and allotriomorphic ferrite, Figure 2.1.

Each colony has to grow to a definite size (R) to reach paraequilibrium, to an extent which is determined by the lever rule:

$$\left(\frac{r}{R}\right)^3 = \frac{V_P}{V_\gamma'} \tag{2-1}$$

where $V_P = \dfrac{\bar{x} - x^{\alpha\gamma}}{x_P - x^{\alpha\gamma}}$ is the pearlite volume fraction, $V_\gamma' = \dfrac{\bar{x} - x^{\alpha\gamma}}{x^{\gamma\alpha} - x^{\alpha\gamma}}$ is the paraequilibrium austenite volume fraction, $\bar{x}$ is average carbon mole fraction in steel, $x^{\alpha\gamma}$ is carbon mole fraction of ferrite in paraequilibrium with austenite, $x^{\gamma\alpha}$ is carbon mole fraction of austenite in equilibrium with

ferrite

When the dimension r equals R, intercirtical annealing can reach paraequilibrim.

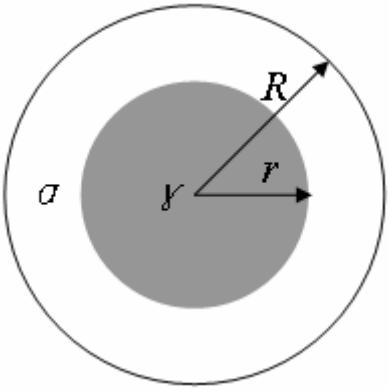

Figure 2.1: Schematic illustration of austenite growth from pearlite colony.

The growth of austenite is assumed to be controlled by carbon diffusion within the austenite, so that the dimension of a given austenite particle will increase parabolically with time. This remains the case prior to soft-impingement, with further reductions in growth rate when there is an overlap of diffusion fields or when the far-field concentration is affected. The method by which soft-impingement is dealt with is described later.

The one-dimensional parabolic rate constant α_1 which is the proportionality constant relating particle dimension to time during isothermal growth, can be calculated using existing theory, for the case where austenite advances into allotriomorphic ferrite [33]. Figure 2.2 shows the carbon concentration profiles in α and γ before and during austenite growth. The austenite must become more dilute in carbon as it grows, with

the rate of interface motion being determined by the diffusion of carbon in the austenite behind the interface. In Figure 2.2, x_γ^I is the initial mole fraction of carbon in the austenite. Given local equilibrium at the interface, the carbon concentration of austenite at the γ/α interface during austenitisation is $x^{\gamma\alpha}$ and that of ferrite is $x^{\alpha\gamma}$. The carbon concentration in austenite far away from the interface is assumed to remain constant at x_γ^I. The coordinate z is normal to the γ/α interface.

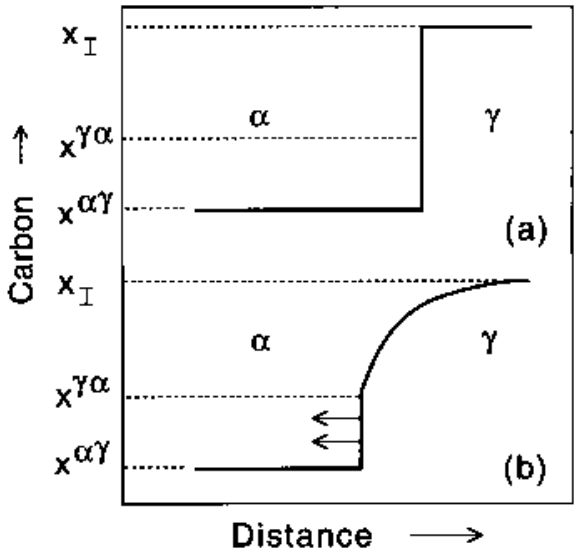

Figure 2.2: Distribution of carbon, (a) before austenitisation from a mixture of ferrite and austenite, and (b) during the growth of austenite. [33]

The flux of carbon in the austenite, towards the γ/α interface, at the position of interface is from Fick's first law given by:

$$J = -D\left\{x^{\gamma\alpha}\right\}\left.\frac{\partial x}{\partial z}\right|_{z=Z} \tag{2-2}$$

The rate at which the carbon concentration of austenite is diluted is

$$R_d = v_d\left(x_\gamma^I - x^{\alpha\gamma}\right) \tag{2-3}$$

where v_d is the velocity of interface (the diffusion-field velocity). Given that

$$Z = \alpha_1 t^{1/2} \tag{2-4}$$

it follows that:

$$v_d = \frac{dZ}{dt} = \frac{1}{2}\alpha_1 t^{-1/2} \tag{2-5}$$

Consequently, the rate at which the carbon concentration of austenite is diluted is given by:

$$R_d = \frac{1}{2}\alpha_1 t^{-1/2}\left(x_\gamma^I - x^{\alpha\gamma}\right) \tag{2-6}$$

Making the approximation that the concentration dependence of the diffusion coefficient of carbon can be represented by its weighted average diffusivity $\overline{D}$ [33], conservation of mass at the interface requires that:

$$\frac{1}{2}\alpha_1 t^{-1/2}\left(x_\gamma^I - x^{\alpha\gamma}\right) = -D\left.\frac{\partial x}{\partial z}\right|_{z=Z} \tag{2-7}$$

This equation expresses the condition that as the austenite becomes dilute as it grows, the change in concentration at the interface is compensated by a diffusion flux of carbon towards the α/γ interface. The differential equation for the matrix is:

$$\frac{\partial x}{\partial t} = \frac{\partial}{\partial z}\left(\overline{D}\frac{\partial x}{\partial z}\right) \tag{2-8}$$

Subject to the boundary conditions $x = x^{\gamma\alpha}$ at $z = Z\{t\}$, and $x = x_{\gamma}^{I}$ at $t = 0$. Its solution leads to the following relationship from which α_1 can be determined [34]:

$$f = \frac{x_{\gamma}^{I} - x^{\gamma\alpha}}{x_{\gamma}^{I} - x^{\alpha\gamma}} = H_1\left\{\overline{D}\right\} \tag{2-9}$$

$$H_1\{\overline{D}\} = \left(\frac{\pi}{4\overline{D}}\right)\alpha_1 \operatorname{erfc}\left\{\frac{\alpha_1}{2\overline{D}^{1/2}}\right\}\exp\left\{\frac{\alpha_1^2}{4\overline{D}}\right\} \tag{2-10}$$

Where: f is a dimensionless supersaturation.

For three-dimensional growth [34, 35]:

$$\left.\begin{aligned} \alpha_3 &= \left(\frac{\pi}{2f}\right)^{1/2}\alpha_1 \qquad & \alpha_1 &\ll 1 \\ \alpha_3 &= 3\alpha_1 & \alpha_1 &\gg 1 \end{aligned}\right\} \tag{2-11}$$

Volume fration of austenite:

$$V_{\gamma} = \left(\frac{Z}{R}\right)^3 V_{\gamma}' \tag{2-12}$$

Soft impingement

The model above is based on the assumption that the carbon concentration far away from the α/γ interface x_{γ}^{I} remains constant, *i.e.*, the extent of the ferrite ahead of the interface is semi-infinite. That obviously is not the

case in practice; soft impingement is the term used to describe the process which leads to a change in the far-field composition. Robson and Bhadeshia suggested the mean field approximation for soft-impingement [36]. In this, solute concentration changes are averaged over the whole of the austenite as a method for dealing with soft-impingement.

$$\overline{x_\gamma} = Z_0 \left(x_\gamma^I - x^{\alpha\gamma} \right) / z + x^{\alpha\gamma} \tag{2-12}$$

2.2 Results and discussion

The chemical compositions of the steel studied are show in table 2.1

Table 2.1: Steel composition, wt%

	C	Mn	Si	Al	P
Ref. steel	0.2	1.5	0.3	0.05	0.005
Si steel	0.2	1.5	1.5	0.05	0.005
Al steel	0.2	1.5	0.3	1.50	0.005
P steel	0.2	1.5	0.3	0.05	0.100
	Nb	Mo	N	S	B
Ref. steel	0.003	0.04	0.003	0.003	0.0005
Si steel	0.003	0.04	0.003	0.003	0.0005
Al steel	0.003	0.04	0.003	0.003	0.0005
P steel	0.003	0.04	0.003	0.003	0.0005

2.2.1 Thermodynamic Calculations

ThermoCalc was used to calculate the equilibrium phase diagram (Figure 2.3) for all four steels. The thermodynamic data base used was *SSOL2*, allowing the following phases to be present: FCC_A1, BCC_A2, CEMENTITE and LIQUID. There is in each case, a pronounced triple phase region between where austenite, ferrite and cementite coexist in equilibrium.

(a)

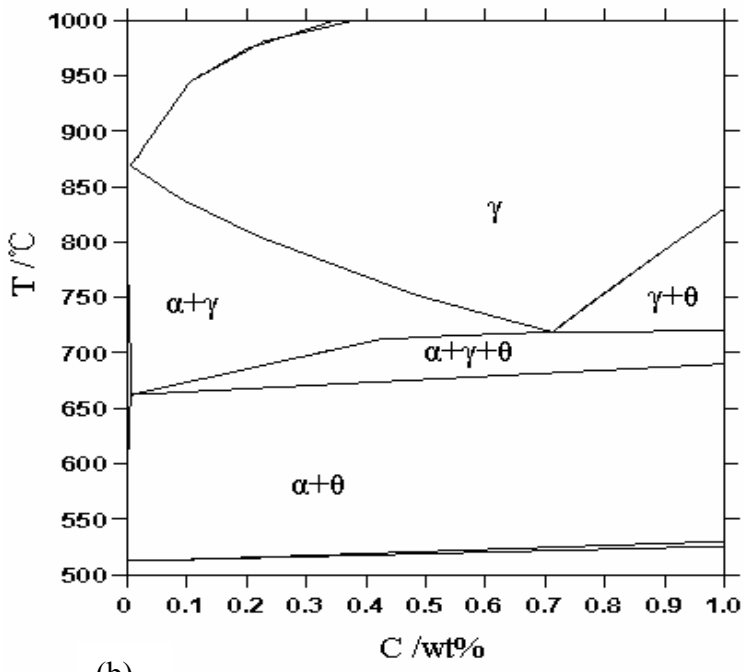
1000
950
900
850
800
750
700
650
600
550
500
T /℃
γ
α+γ
γ+θ
α+γ+θ
α+θ
0
0.1
0.2
0.3
0.4
0.5
0.6
0.7
0.8
0.9
1.0
C /wt%

(b)

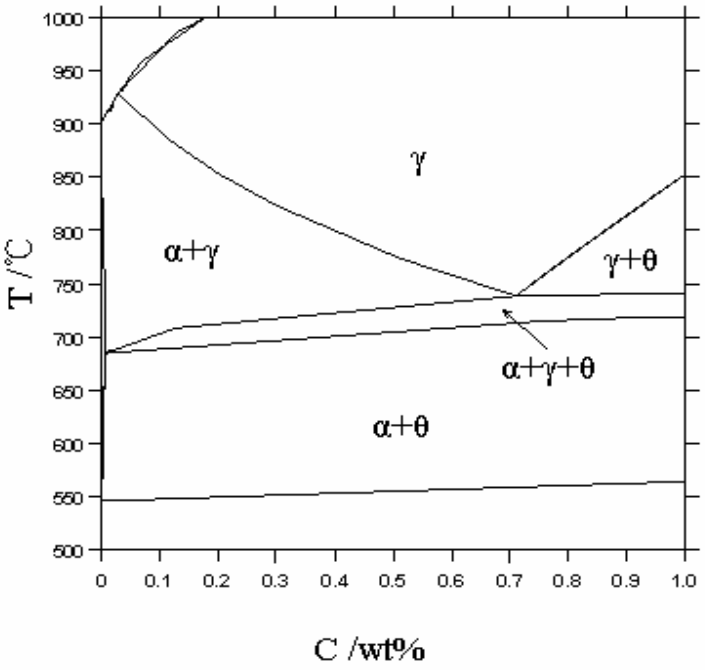
1000
950
900
850
800
750
700
650
600
550
500
T /℃
γ
α+γ
γ+θ
α+γ+θ
α+θ
0
0.1
0.2
0.3
0.4
0.5
0.6
0.7
0.8
0.9
1.0
C /wt%

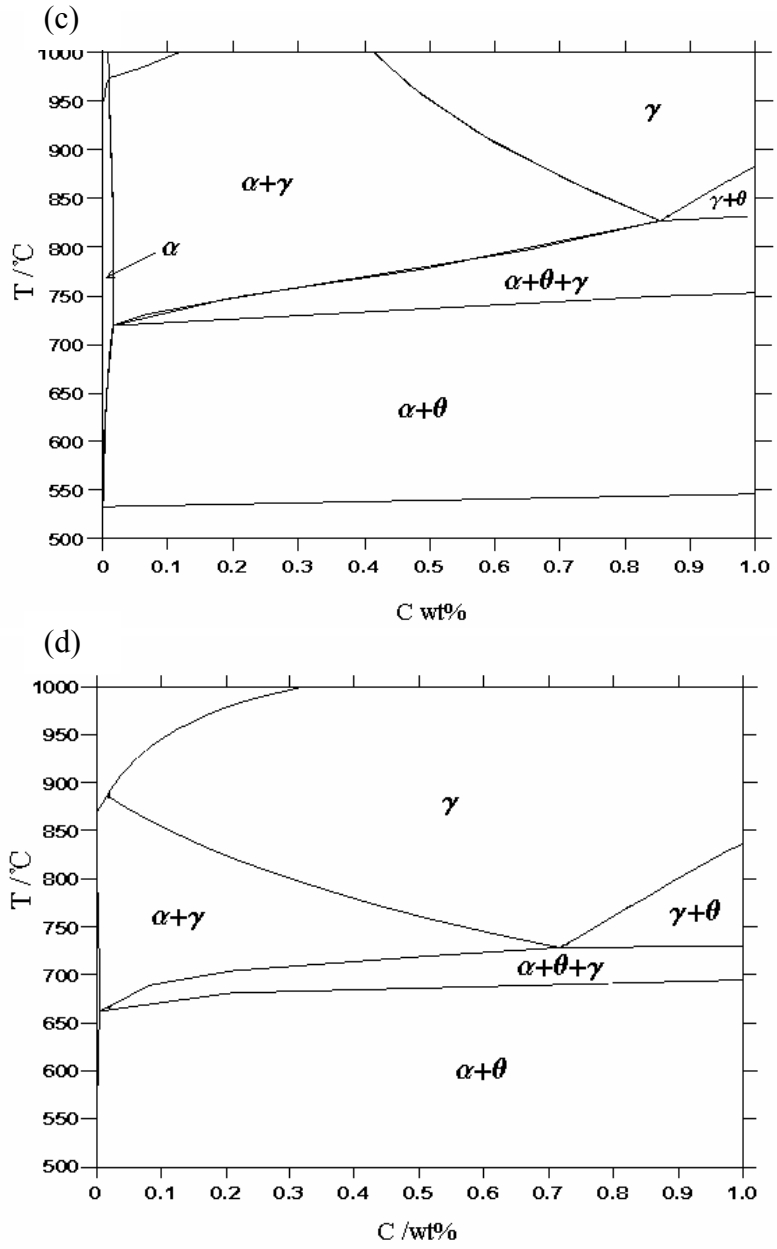

Figure 2.3: Equilibrium phase diagrams. (a): Ref. steel, (b) Si steel, (c) Al steel, (d) P steel.

MTDATA software was used to calculate the Ae_1' and Ae_3' temperatures of the four steels and the variation of phase distribution with temperature. The calculations used *MTDATA* version 4.74 and the MTSOL: NPL Alloy Solution Database version 1.1, 27 March 2000. The phases permitted to exist were FCC_A1, BCC_A2, and CEMENTITE. All substitutional solutes except Si, Al and P were forced into paraequilibrium.

Calculated Ae_1' and Ae_3' temperatures are shown in table 2.2. The Ae_1' temperature is taken as the temperature above which austenite first appears on heating. In Ref. steel, Ae_1' is 702 ℃ and Ae_3' is 810 ℃ for 0.2 wt% carbon. The addition of Si gives increases these temperatures to 716 ℃ and 854 ℃ respectively. The substitution of Si by Al has a pronounced influence on the critical temperatures, with Ae_1' increased to 748 ℃, and the disappearance of the fully austenitic region. That is to say, it becomes impossible to completely austenitise the alloy. For steel P, Ae_1' is 704 ℃ and Ae_3' is 823 ℃.

Table 2.2: Ae_1' and Ae_3' temperature (paraequilibrium calculation) in ℃

	Ae_1'	Ae_3'
Ref. steel	702	810
Si steel	716	854
Al steel	748	N/A
P steel	704	823

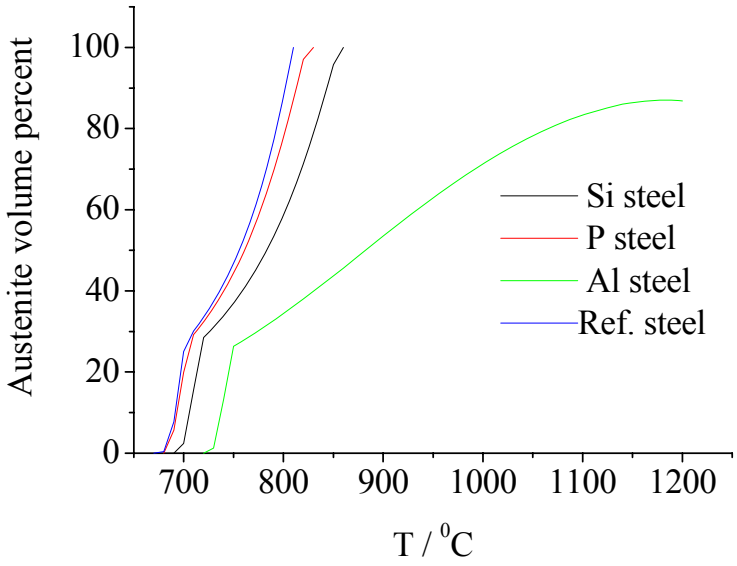

Figure 2.4: Volume percent of austenite as a function of temperature (paraequilibrium calculations).

Figure 2.4 shows the volume fraction of austenite as a function of temperature; all the four steels show a rapid increase in austenite volume fraction as temperature increases, in the early stage, and a slow increase rate after that critical point. That is because of the cementite dissolution, as shown in Figure 2.3, there is a triple phase region, where ferrite, austenite and cementite are in paraequilibrium, when cementite dissolves, large amount of carbon has to be accommodated in the steel, that high carbon region transforms to austenite, leads to a rapid increase in austenite volume fraction.

2.2.2 Kinetic Calculations

The pearlite colony size before heat treatment was found to be around 5 to 30 μm by measure in micrograph from literatures [37-39]. Diffusivity is calculated by the subroutine *MAP_STEEL_DIFFUS* [40-42]. It is highly dependant on temperature, and on the carbon concentration and solute in steel. As austenitisation proceeds, the carbon in austenite decreases, leads to the decrease in diffusivity as shown in Figure 2.5.

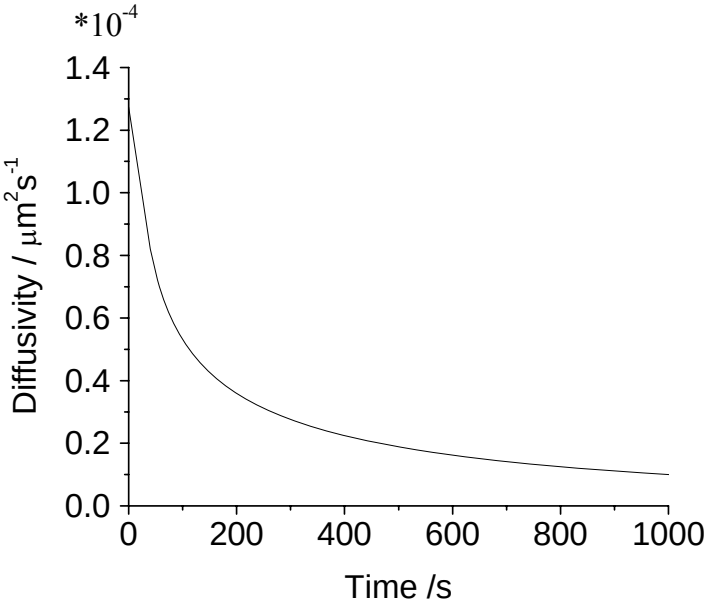

Figure 2.5: Diffusivity as a function of intercritical annealing time (Ref. steel, 775 ℃).

The three-dimensional thickening rate constant $\alpha 3$ decreases as intercritical annealing progresses, is shown in Figure 2.6. This is a result of the decrease in driving force as the carbon concentration approaches paraequilibrium.

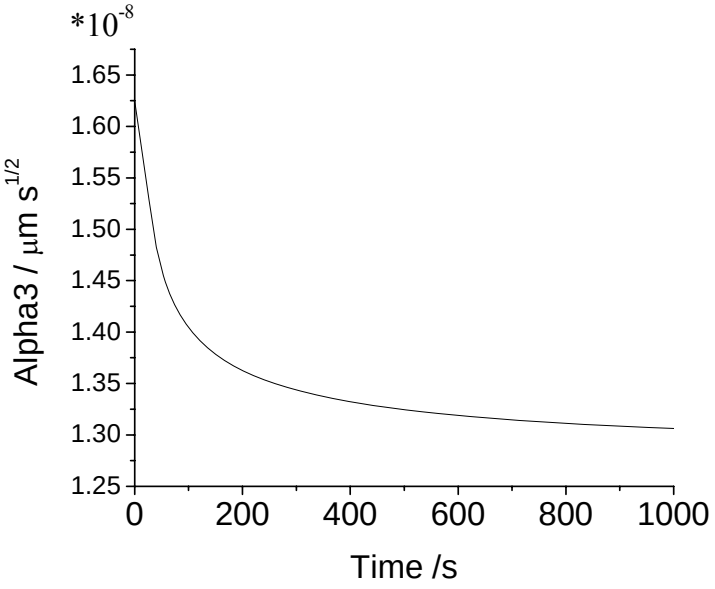

Figure 2.6: $\alpha 3$ as a function of intercritical annealing time (Ref. steel, 775 ℃).

Figure 2.7 shows the α/γ interface velocity during isothermal austenisation. At first the supersaturation is high resulting in a large velocity. As the austenite grows, its carbon concentration decreases, thereby leading to a reduction in supersaturation. The motion of interface therefore slows down. When the amount of austenite approaches the paraequilibrium fraction, the boundary velocity asymptotically approaches zero.

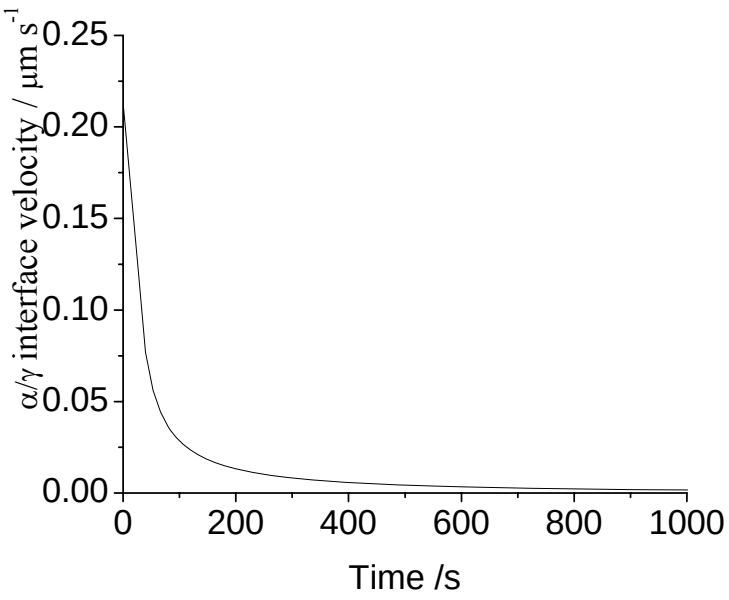

Figure 2.7: α / γ interface velocity as a function of intercritical annealing time (Ref. steel, pearlite colony size 10 μm , 775 ℃).

To examine the effects of soft-impingement, calculations were done with and without implementing changes in the far-field concentration, as shown in Figure 2.8. It is clearly shown that soft-impingement has a large effect and should not be neglected in any calculation. Figure 2.8 also shows the case for three-dimensional growth, which naturally is much much faster than one-dimensional growth.

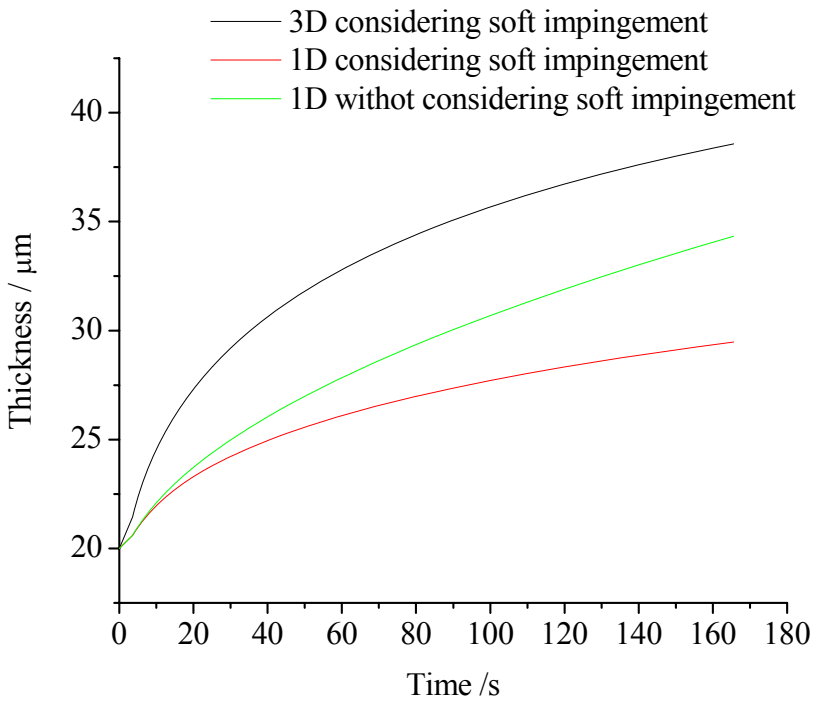

Figure 2.8: Comparison of one-dimensional three-dimensional and soft-impingement effects (Ref. steel, pearlite colony size 20 μm , 775 ℃).

2.2.2.1 Influence of chemical composition

For all the four steels intercritically annealed at 775 ℃ and for a pearlite colony size of 10 μm , the calculated austenite volume fraction shown in Figure 2.9. The kinetics of austenite formation are similar for the Ref. and P steels, both taking a long time to reach paraequilibrium, particularly when compared against the Al steel. The Si steel is intermediate. As shown in Figure 2.3, the Al steel cannot be fully austenised, and has a broad $\alpha+\gamma$ two-phase zone which means that the paraequilibrium austenite volume

fraction is much smaller than all the other alloys.

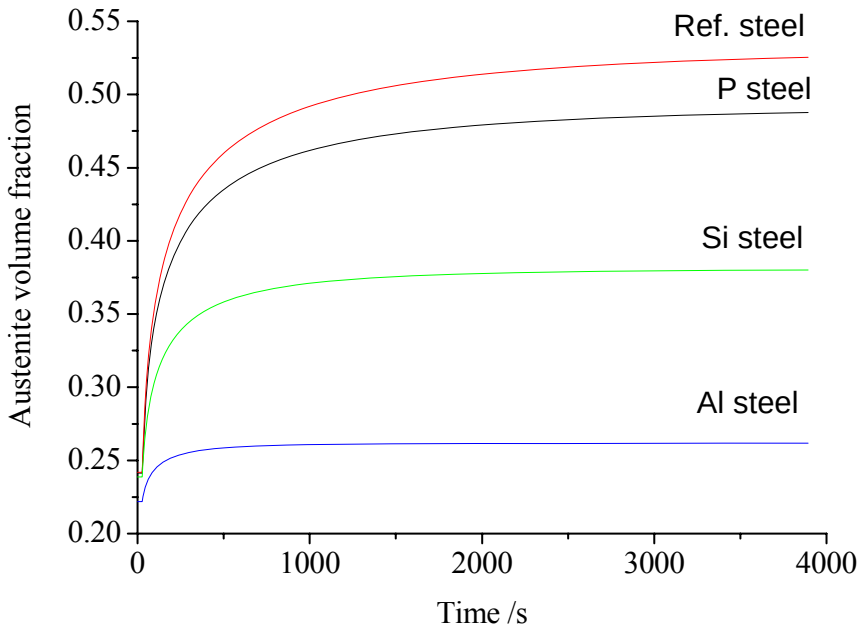

Figure 2.9: Austenite volume fraction as a function of time (Pearlite colony size: 10 μm , 775 ℃).

For carbon concentration evolution, Figure 2.10 shows Al steel has the highest carbon concentration at a same annealing temperature, and reaches paraequilibrium fairly rapidly. Si steel reaches paraequilibrium slower, but Ref. steel and P steel are even slower, showing similar tendencies.

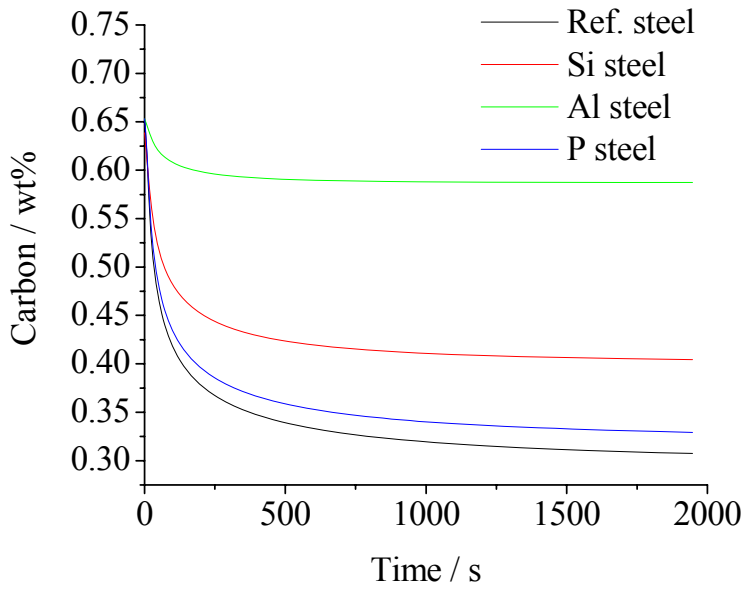

Figure 2.10: Carbon concentration in austenite as a function of time (Pearlite colony size: 10 μm , 775 ℃).

2.2.2.2 Influence of the starting microstructure

The influence of the starting microstructure is examined by assuming different pearlite colony sizes, as illustrated in Figure 2.11.

Al steel intercritical annealing at 775℃, austenite equilibrium volume fraction is 0.2475, for pearlite colony size 5 μm , it takes about 250 s to reach equilibrium; for 10 μm , it takes more than 500 s to reach equilibrium; for 20 μm and 30 μm , it takes more than 2000 s to reach equilibrium.

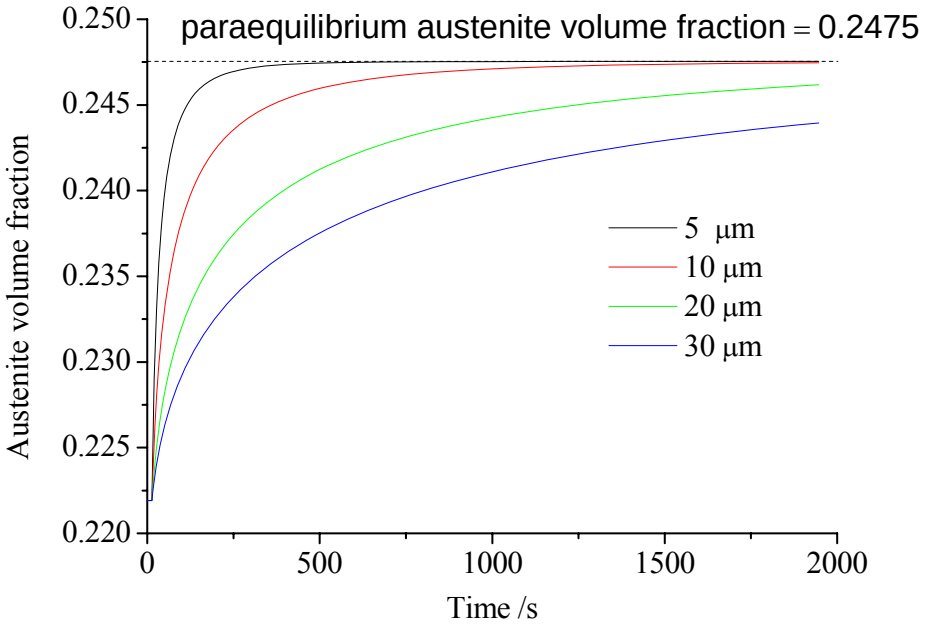

Figue 2.11: Influence of pearlite colony size on austenite formation (Al steel intercritically annealed at 775℃).

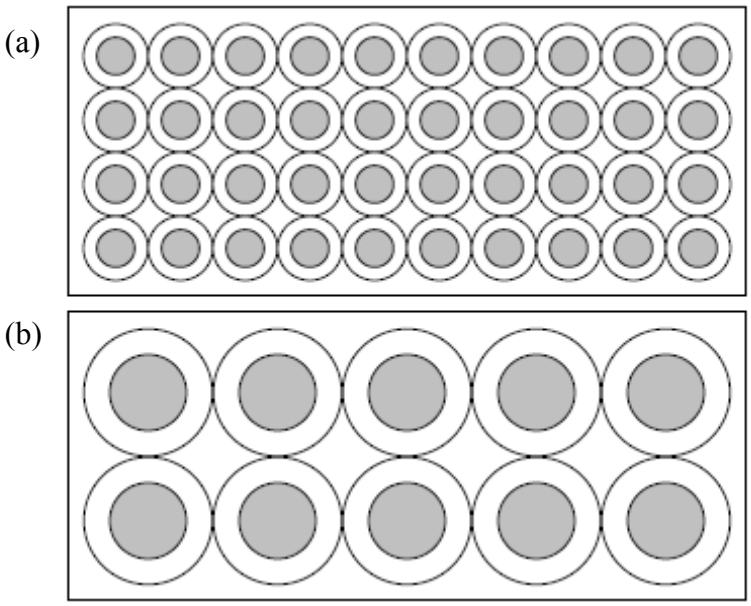

Figure 2.12: Schematic illustration of pearlite size effect on austenisation.

Pearlite colony size influences the kinetic of austenisation by they role as potential austenite nuclei. According to thermodynamics, the pearlite volume fraction is fixed by the steel composition. When the pearlite colony size is small, there will be more pearlite colonies, as show in Figure 2.12, the shadowed areas in (a) and (b) are identical, but particles in (a) have a radius half of that in (b), so the colony number in (a) is four times that of (b). When they grow to paraequilibrium, the particles in (b) obviously have to grow through longer distances.

2.2.2.3 Influence of intercritical annealing temperature

Temperature influences the kinetics of intercritical annealing through its effect on carbon diffusivity and the driving force for austenite formation. Higher temperatures leads to larger carbon diffusivity and larger driving force for austenite formation. At higher intercritical annealing temperatures, the paraequilibrium volume fraction of austenite is larger.

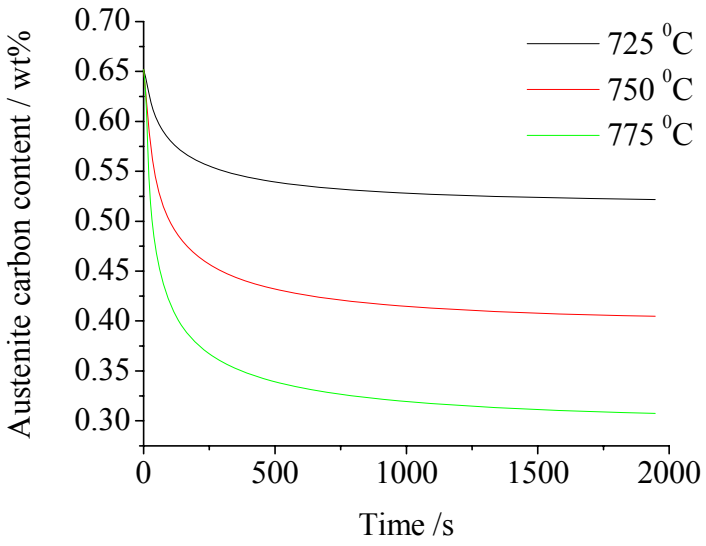

Figure 2.13: Ref. steel austenite carbon content as a function of time (Intercritical annealed at 725, 750 or 775 ℃, pearlite colony size 10 μm).

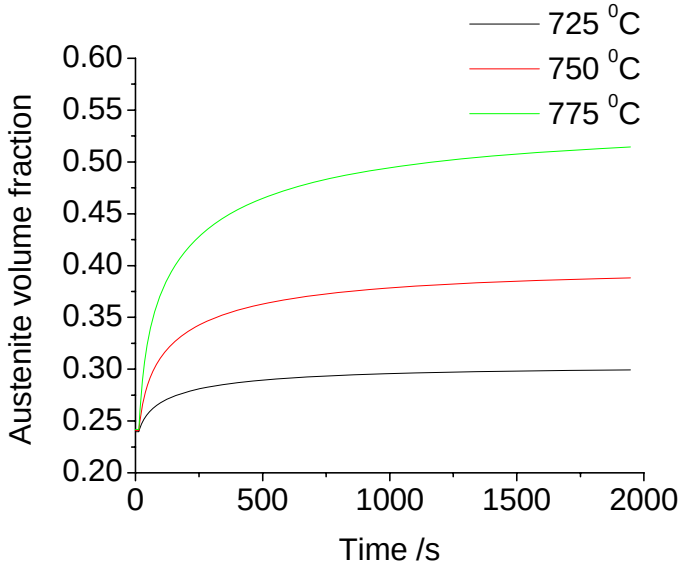

Figure 2.14: Ref. steel austenite volume fraction as a function of time (Intercritical annealed at 725, 750 or 775 ℃, pearlite colony size 10 μm).

In Figure 2.13, Ref. steel reaches paraequilibrium faster at 725 ℃ than 750 ℃ or 775 ℃, that may comes from the paraequilibrium carbon concentration is much smaller that of annealed at 750 ℃ or 775 ℃. It is more clearly shown in Figure 2.14, for the volume fraction of austenite. The tendencies for Si steel and P steel are very similar. However, the scenario is different for the Al steel shown in Figure 2.17 and 2.18, for it cannot be fully austenitised in this carbon concentration range. The same increment in intercritical annealing temperature in the Al steel leads only to a smaller change in paraequilibrium carbon concentration of austenite than all the other three steels. The curves for 750 ℃ in Figure 2.17 and 2.18 are rather flat, because the temperature is close to Ae_1'.

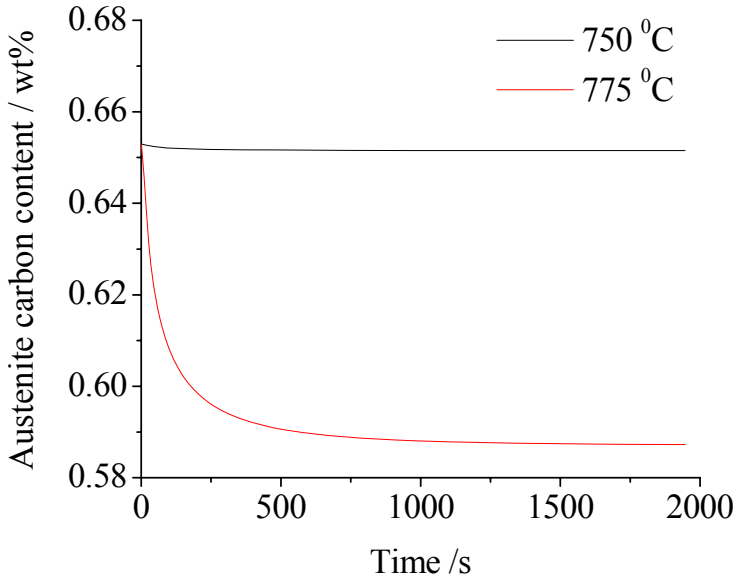

Figure 2.17: Al steel austenite carbon content as a function of time. (Intercritical annealed at 725, 750 or 775 ℃, pearlite colony size 10 μm).

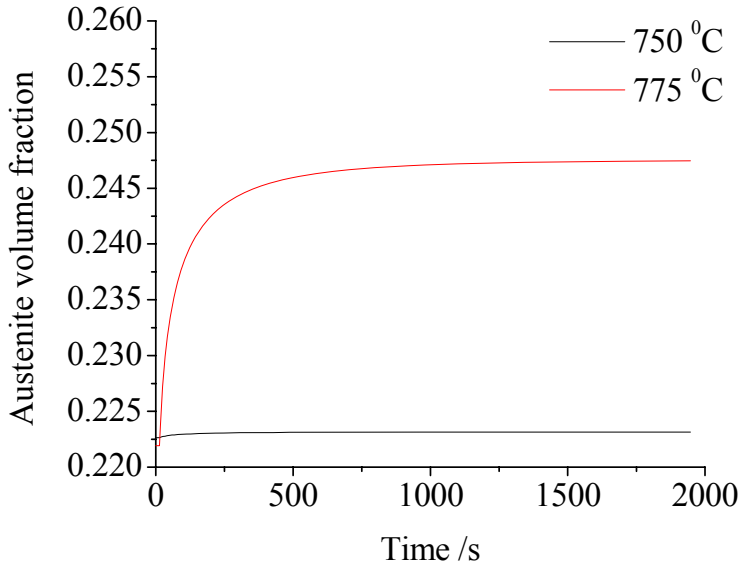

Figure 2.18: Al steel austenite volume fraction as a function of time (Intercritical annealed at 725, 750 or 775 ℃, pearlite colony size 10 μm).

All the calculations show that in a typical intercritical annealing time of about 3-5 minutes [43, 44] , the steel will not be able to reach paraequilibrium, which is quite surprising since this is what is often assumed [32].

2.3 Summary

Paraquilibrium thermodynamic calculations show that the substitution of Si by P has little effect on Ae_1' and Ae_3' transformation temperatures over the concentration ranges investigated. The replacement of Si by Al, however, shifts these temperatures to appreciably higher values and can eliminate the

ability of the steel to fully austenitise. A small amount of P addition has little influence on those temperatures.

The pearlite colony size has a large influence on the time required to reach paraequilibrium during intercritical annealing. A small pearlite colony size is conducive to faster austenitisation because there will then be a larger number density of particles which have to grow through smaller distances. Equilibrium can be achieved much faster than with larger colony sizes, because the pearlite volume fraction is constant. A small size means a larger number density of colonies, which act as nuclei for austenisation.

Paraquilibrium will not be reached in typical intercritical annealing processes. Refinement of the microstructure during the cold rolling process shows accelerated austenisation during intercritical annealing.

III Modeling of isothermal bainite transformation

There are two different points of view on the kinetics of the bainite transformation. One is diffusion controlled growth [45-47]; and the other is a displacive transformation mechanism [48]. Therefore, there are two corresponding approaches to model the rate of the reaction [49]. These two approaches are scheduled, but due to time limitations, the displacive mechanism has not get investigated been done yet, so only the diffusion controlled growth model of the bainitic plates will be presented.

Since the bainite transformation proceeds by a nucleation and growth mechanism, the overall reaction rate depends on the driving force and the atomic mobility resulting in a C-curve nature of the time-temperature-transformation (TTT) diagram. Although the transformation completes when cementite formation is allowed to occur, it is essential to treat the formation of bainitic ferrite and cementite individually and allow them to compete with each other to cope with the large variety of alloy compositions that are adopted in industry.

3.1 Construction of Bainite Transformation Model

A typical TTT diagram for steel is shown in Figure 3. The incubation time is that required to obtain a measurable extent of transformation. In present work, the model deals with bainite growth.

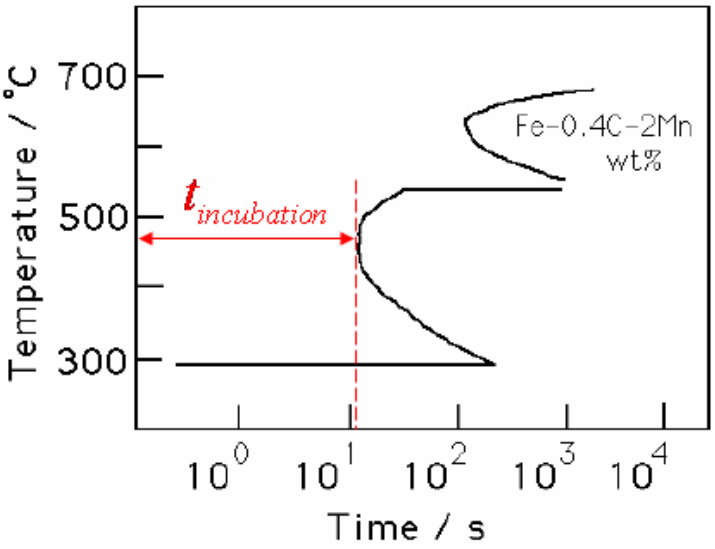

Figure 3.1: Schematic illustration of TTT diagram [50].

Bainite growth is assumed to occur in an edgewise manner [51], the longitudinal growth rate is much faster than that in the transverse direction. The following assumptions are made to deal with this:

1) At the end of the incubation time, two bainite plates with infinitesimal thickness are formed, as shown in Figure 3.2, and they then thicken due to carbon diffusion into the surrounding austenite.
2) Local paraequilibrium is held at the bainite/austenite interface.
3) The thickening of bainite plates is carbon diffusion-controlled.

The initial composition in the context of TRIP-assisted steel is the austenite composition after intercritical annealing, which is obtained using the intercritical annealing model.

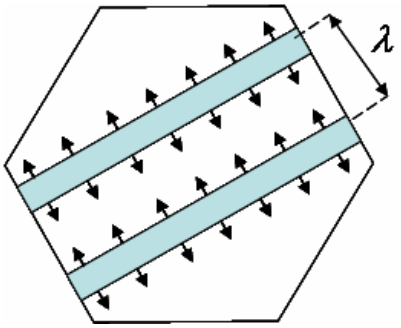

Figure 3.2: Schematic illustration of the geometry of bainite plates.

The temperature of bainitic isothermal heat-treatment in TRIP-assisted steel normally is 300℃ to 450℃ [43, 52-54]. In this temperature range and within the time scales involved, substitutional solutes can't diffuse, although carbon partitions, leading to the paraequilibrium state.

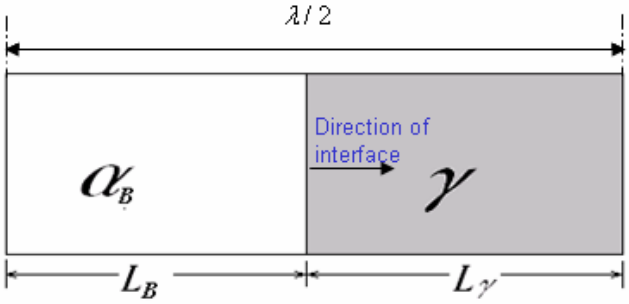

Figure 3.3: Schematic illustration of bainite growth.

Assuming the interplate spacing is λ, because of the geometric symmetry, only half of the interplate spacing needs to be modeled, as shown in Figure 3.3.

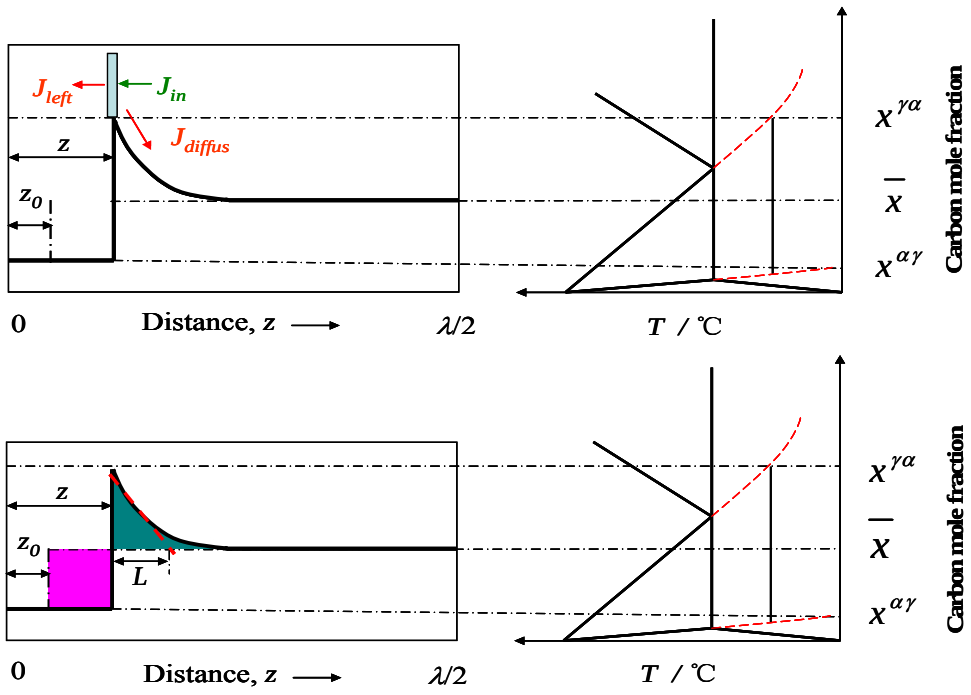

Figure 3.4: schematic illustration of carbon concentration and interface motion.

At the bainite-austenite interface, there are three fluxes, as illustrated in Figure 3.4, J_{letf} , J_{in} due to the movement of the interface; and J_{diffus} due to the carbon concentration gradient in austenite. The paraequilibrium carbon concentrations in austenite and bainite are calculated by extrapolating Ae_3' and $\alpha/\alpha+\gamma$ boundaries respectively.

$$J_{out} = J_{left} + J_{diffus} = x^{\alpha\gamma}\frac{dz}{dt} - D\frac{dx^{\gamma}}{dz}\bigg|_i \tag{3-1}$$

$$J_{in} = x^{\gamma\alpha}\frac{dz}{dt} \tag{3-2}$$

where, $x^{\gamma\alpha}$ is carbon concentration in austenite which is in paraequilibrium with bainitic ferrite;

$x^{\alpha\gamma}$ is carbon concentration in bainitic ferrite which is in paraequilibrium with austenite;

D is the carbon diffusivity in austenite;

$\left.\frac{dx^{\gamma}}{dz}\right|_i$ is the carbon concentration gradient in austenite at the interface.

To maintain local paraequilibrium at the interface, it is necessary for:

$$J_{in} = J_{out} \tag{3-3}$$

so that, $$\frac{dz}{dt} = -\frac{D}{x^{\gamma\alpha} - x^{\alpha\gamma}} \left.\frac{dx^{\gamma}}{dz}\right|_i \tag{3-4}$$

There will eventually be a situation when soft-impingement occurs and the far field concentration in austenite increases, as shown in Figure 3.5.

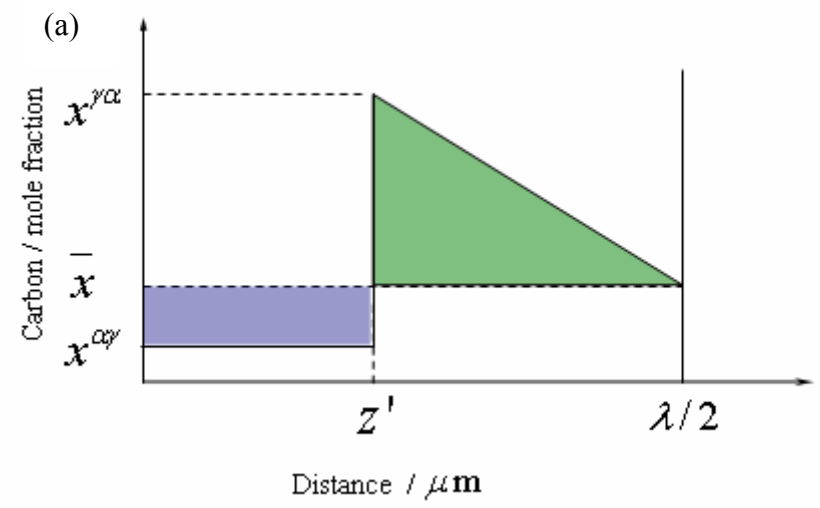

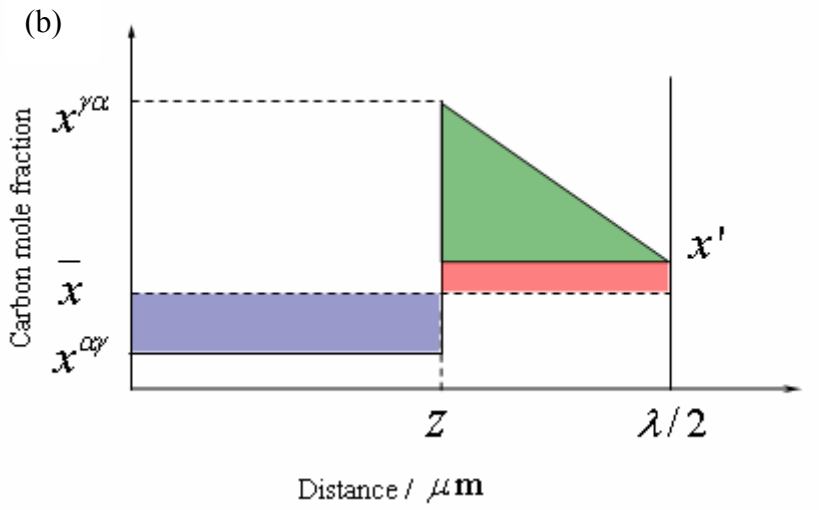

Figure 3.5: illustration of carbon diffusion field. (a): Critical diffusion field length, (b): Increase of the far field concentration of carbon in austenite, corresponding to soft-impingement

z' is the interface position when the diffusion field length reaches critical value.

when $0 < z < z'$

$$\left.\frac{dx^{\gamma}}{dz}\right|_{i} = -\frac{x^{\gamma\alpha} - \bar{x}}{L} \tag{3-5}$$

where L is the length of diffusion field. Mass conservation gives:

$$(\bar{x} - x^{\alpha\gamma})z = (x^{\gamma\alpha} - \bar{x})\frac{L}{2} \tag{3-6}$$

Inserting (3-5) and (3-6) to (3-4), and integrating (3-4) gives:

$$z = z_0 + \frac{x^{\gamma\alpha} - \bar{x}}{\sqrt{(\bar{x} - x^{\alpha\gamma})(x^{\gamma\alpha} - x^{\alpha\gamma})}}\sqrt{Dt} \tag{3-7}$$

where Z_0 is the starting bainite/austenite interface position, in this context

it is zero.

when $z > z'$

$$\left.\frac{dx^{\gamma}}{dz}\right|_{i} = -\frac{x^{\gamma\alpha} - x'}{\frac{\lambda}{2} - z} \tag{3-8}$$

mass conservation gives:

$$(\bar{x} - x^{\alpha\gamma})z = \frac{(x^{\gamma\alpha} - x')\left(\frac{\lambda}{2} - z\right)}{2} + (x' - \bar{x})\left(\frac{\lambda}{2} - z\right) \tag{3-9}$$

Inserting (3-8) and (3-9) to (3-4) we obtain:

$$dz = D\frac{2x^{\gamma\alpha}\left(\frac{\lambda}{2} - z\right) - \lambda\bar{x} + 2x^{\alpha\gamma}}{(x^{\gamma\alpha} - x^{\alpha\gamma})\left(\frac{\lambda}{2} - z\right)^{2}}dt \tag{3-10}$$

3.2 Construction of Cementite Precipitation Model

Cementite is a detrimental phase in TRIP steel, it is important to know how it forms, and to control it. As is well know Si has a great influence on the kinetics of cementite formation, so it is used in TRIP steels to retard cementite precipitation. The model developed in this work is to investigate how Si affects cementite transformation.

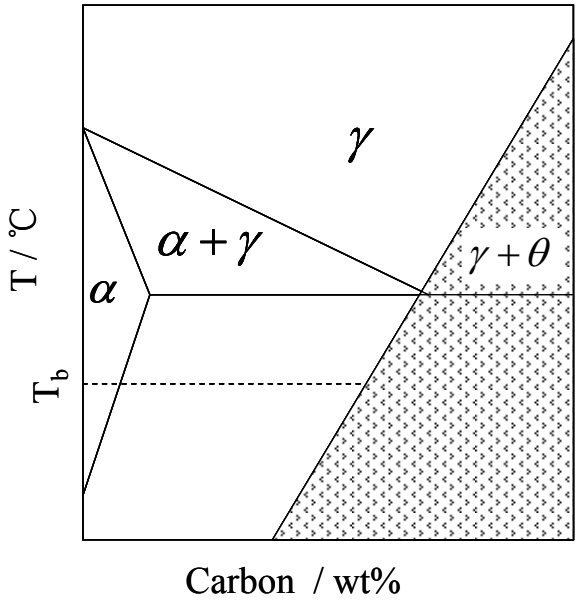

Figure 3.6: Thermodynamic condition for cementite precipitation from austenite [55].

For cementite to precipitate from austenite, it has to satisfy the thermodynamic condition shown in Figure 3.6. When the carbon concentration in austenite exceeds the extrapolated A_{cm} line, at the bainite holding temperature, it becomes thermodynamically possible to precipitate cementite; in the diffusion-controlled growth model this condition is

thermodynamically satisfied below the eutectoid temperature, but kinetically many other factors may need to be taken into account.

Figure 3.7 shows the driving force of transformation from austenite to cementite.

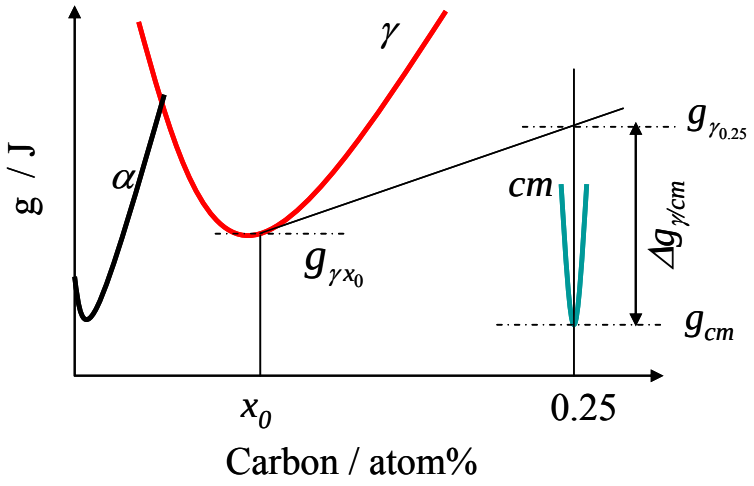

Fugure 3.7: schematic illustration of driving force of transformation from austenite to cementite. $g_{\gamma x_0}$ is Gibbs free energy of austenite per atom with carbon mole fraction of x_0, g_{cm} is Gibbs free energy of cementite per atom, $g_{\gamma/cm}$ is the driving force of transformation from austenite to cementite, $g_{\gamma_{0.25}}$ is the Gibbs free energy of austenite per atom with carbon mole fraction of 0.25.

The free energy per iron atom of austenite with the same carbon concentration of cementite can be expressed as:

$$g_{\gamma 0.25} = g_{\gamma x_0} + (0.25 - x_0)\left.\frac{dg_\gamma}{dx}\right|_{x_0} \tag{3-11}$$

where: x_0 is average austenite carbon mole fraction;

$g_{r0.25}$ is the free energy per atom of austenite with 0.25 mole fraction of carbon;

$g_{\gamma x0}$ is the free energy per atom of austenite with the original carbon concentration x_0.

The driving force for nucleation per iron atom is:

$$\Delta g_{\gamma/cm} = g_{cm} - g_{\gamma 0.25} \tag{3-12}$$

The unstable carbon cluster has two competitive ways to reduce its energy. The first is carbon diffusion away driven by its concentration gradient; if this occurs first, the cluster (*i.e.* the embryo of cementite) collapses; the other is iron atoms transform to cementite lattice driven by $\Delta g_{\gamma/cm}$; if this occurs first, a cementite nucleus forms.

From classical nucleation theory, nucleation rate is given by:

$$I = AN_0 \exp(-Q_C / kT) \exp(-G^* / kT) \tag{3-13}$$

where: A is an attempt frequency,

N_0 is the number density of nucleation sites,

Q_C is an activation energy for transforming atom from the matrix to the cementite,

$G^* = (4\eta^3\delta^3)/[27(\Delta g_{\gamma/cm})^2]$ is the critical energy for nucleation.

When Si is present in cementite, the rate of the process is controlled by Si diffusion in the matrix if Si partitions. But the diffusivity of Si is significantly smaller than that of carbon, so it cannot partition during the

process. Thus, Si partitioning is impossible kinetically at the temperature where bainite forms. The free energy of Si modified cementite is shown in Figure 3.8. It can be expressed as:

$$g'_{cm} = g_{cm} + x_{Si}\Delta g_b - kT[(1-x_{Si})\ln x_{Si} + x_{Si}\ln x_{Si}] \approx g_{cm} + x_{Si}\Delta g_b \quad (3\text{-}14)$$

Where: x_{Si} is the mole fraction of Si,

Δg_b is the energy difference due to introduction of Si.

So the driving force for forming a Si-modified cementite nucleus is:

$$\Delta g'_{\gamma/cm} = g_{\gamma 25} - g'_{cm} = \Delta g_{\gamma/cm} - x_{Si}\Delta g_b \quad (3\text{-}15)$$

The critical free energy for the Si-modified cementite nucleation is:

$$G'^* = (4\eta^3\delta^3)/[27(\Delta g_{\gamma/cm} - x_{Si}\Delta g_b)^2] \quad (3\text{-}16)$$

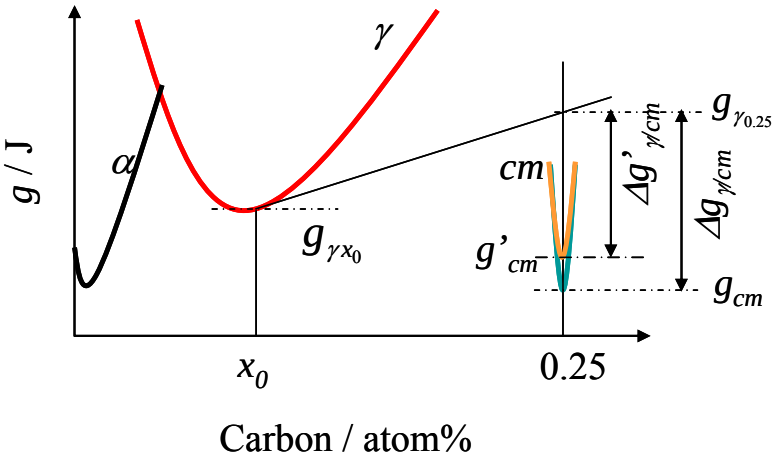

Figure 3.8: Schematic illustration of cementite Gibbs free energy changes by adding Si.

The nucleation rate of Si-modified cementite is:

$$I' = AN_0 \exp(-Q_C/kT)\cdot\exp(-G'^*/kT) \quad (3\text{-}17)$$

The ratio of cementite nucleation rate of Si-modified cementite and Si-free cementite can be express as follow:

$$\begin{aligned} R_I &= I'/I \\ &= \exp\{-(G^*/kT)[1/(1-x_{Si}\Delta g_b/\Delta g_{\gamma/cm})^2 - 1]\} \end{aligned} \tag{3-18}$$

Assuming $\Delta G^* = kT$, R_I changes with respect to $x_{Si}\,\Delta g_b/\Delta g_{\gamma/cm}$ as shown in Figure 3.9.

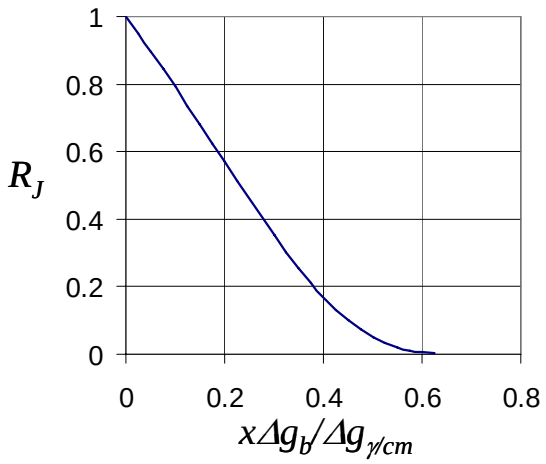

Figure 3.9: Nucleation ratio changes with respect to Si concentration.

The grow rate of cementite handled by Zener's model of one-dimensional diffusion controlled growth [34]:

$$v = \frac{1}{2}B\left(\frac{D}{t}\right)^{1/2} \tag{3-19}$$

where B is a constant.

Overall transformation volume fraction of cementite was treated by Avrami equation [56-58], for a spherical nucleus it is:

$$V_{cm} = 1 - \exp(-C\pi I v^3 t^n) \tag{3-20}$$

where V_{cm} is the fraction of cementite formed at time t over the equilibrium cementite volume, C is a constant. Back-calculation will be necessary to find a value for C and n.

3.3 Combination of the bainite plate growth and cementite precipitation model

When cementite precipitates, carbon is consumed, and the bainite transformation can go further. To take this into account, a combination of the bainite model and cementite model is important.

Consider cementite precipitation, mass conservation for carbon will change to:

when $0 < z < z'$

$$(\bar{x} - x^{\alpha\gamma})z = (x^{\gamma\alpha} - \bar{x})\frac{L}{2} + P \tag{3-21}$$

where P is total carbon in mole fraction consumed by cementite precipitation.

Insert (3-5) and (3-21) to (3-4), then integrate (3-4) gives:

$$z = z_0 + \frac{P + \sqrt{P^2 + \frac{(\bar{x} - x^{\alpha\gamma})(x^{\gamma\alpha} - \bar{x})^2}{(x^{\gamma\alpha} - x^{\alpha\gamma})} Dt}}{(\bar{x} - x^{\alpha\gamma})} \tag{3-22}$$

When $z' < z < \frac{\lambda}{2}$

$$(\bar{x} - x^{\alpha\gamma})z = \frac{(x^{\gamma\alpha} - x')\left(\frac{\lambda}{2} - z\right)}{2} + (x' - \bar{x})\left(\frac{\lambda}{2} - z\right) + P \tag{3-23}$$

so:

$$x' = \frac{\bar{x}\lambda - 2x^{\alpha\gamma}z - x^{\gamma\alpha}\left(\frac{\lambda}{2} - z\right) - 2P}{\left(\frac{\lambda}{2} - z\right)} \tag{3-24}$$

insert (3-8) and (3-24) to (3-4) lead to:

$$dz = \frac{(x^{\gamma\alpha} - x')}{(x^{\gamma\alpha} - x^{\alpha\gamma})\left(\frac{\lambda}{2} - z\right)} Ddt \tag{3-25}$$

Total amount of carbon can transform to cementite is: $\frac{\lambda}{2}(x^{\gamma\alpha} - x^{\alpha\gamma})$

So $$P = \frac{\lambda}{2}(x^{\gamma\alpha} - x^{\alpha\gamma})V_{cm} \tag{3-26}$$

3.4 Results and Disscusion

Typical microstructural observations show that the bainite interplate spacing is found to be around 1 μm [4, 59, 60]. In this calculation bainite interplate spacing is set to 1 μm .

Figure 3.10 shows the extrapolated extrapolated $\alpha / \alpha + \gamma$ boundary and Ae_3' line of these four steels. The calculations used *MTDATA* version 4.74 and the MTSOL: NPL Alloy Solution Database version 1.1, 27 March 2000. The phases permitted to exist were FCC_A1, BCC_A2. All substitutional solutes were forced into paraequilibrium. Carbon concentration in austenite is high, at 400 ℃, it can reach more than 3 wt%, Not much difference can be found for these four different steels, and meanwhile in ferrite carbon concentration is low, Al steel has the highest boundary concentration of carbon in ferrite while Si steel has the lowest; almost no noticeable difference can be found between Ref. steel and P steel, and their curves are overlapped.

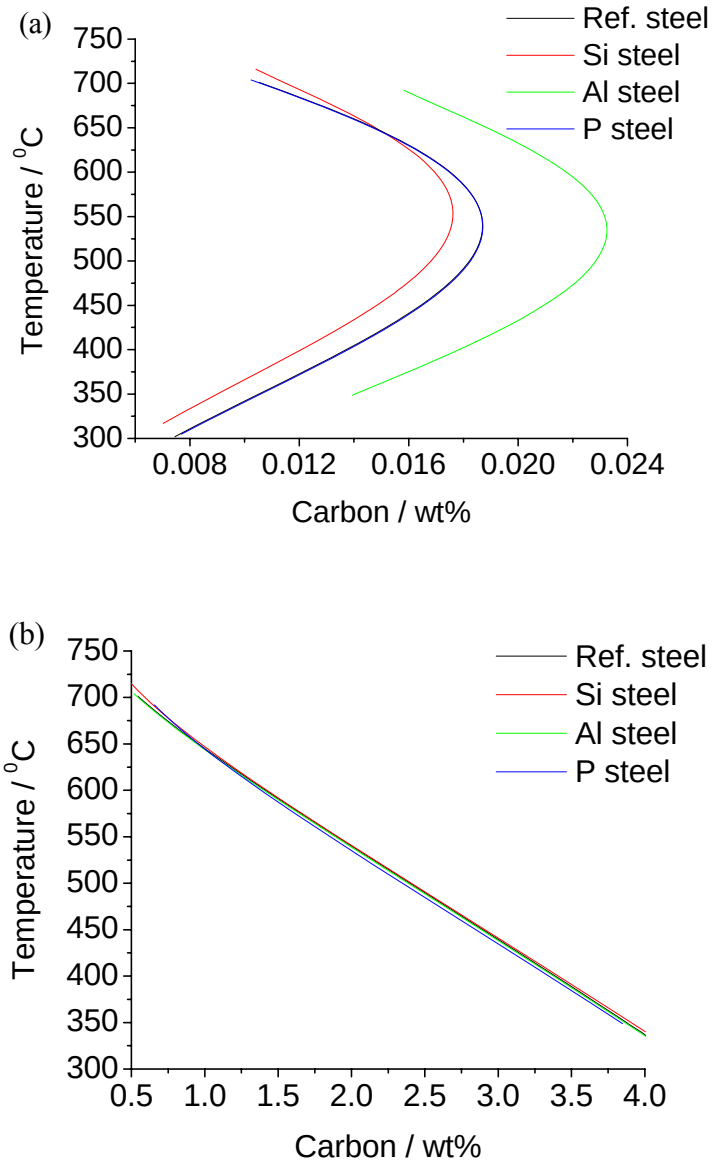

Figure 3.10: Extrapolated paraequilibrium $\alpha / \alpha + \gamma$ boundary and Ae_3' line. (a) $\alpha / \alpha + \gamma$ boundary (b) Ae_3' line (paraequilibrium calculations after intercritical annealing at 760℃).

3.4.1 Influence of chemical composition

For the calculations, the input parameters are $\Delta g_b = 2 \times 10^{-18}$ $B = 1 \times 10^{-8}$ $n = 2$ composition from intercritical annealing, which is listed in table 3.1 and 3.2.

Table 3.1: Composition of austenite after intercritical annealing at 775 ℃(wt%).

	C	Mn	Si	Al	P
Ref.	0.30	1.89	0.27	0.038	0.003
Si	0.40	2.14	1.34	0.033	0.003
Al	0.66	2.60	0.30	0.81	0.0021
P	0.32	1.97	0.28	0.037	0.057
	Nb	Mo	N	S	B
Ref.	0.003	0.035	0.0044	0.0035	0.0002
Si	0.003	0.035	0.0055	0.0038	0.0002
Al	0.004	0.039	0.0089	0.0046	0.0002
P	0.003	0.036	0.0047	0.0036	0.0002

Table 3.2: Composition of austenite after intercritical annealing at 750 ℃(wt%).

	C	Mn	Si	Al	P
Ref.	0.40	2.22	0.26	0.03	0.002
Si	0.49	2.41	1.30	0.03	0.002
Al	0.69	2.70	0.30	0.79	0.002
P	0.42	2.29	0.27	0.03	0.045
	Nb	Mo	N	S	B
Ref.	0.003	0.035	0.006	0.004	0.0002
Si	0.003	0.036	0.006	0.004	0.0002
Al	0.004	0.040	0.009	0.005	0.0002
P	0.003	0.036	0.006	0.004	0.0002

The composition of a steel can greatly influence in transformation behavior, as it is well known that a large amount of Si can retard the cementite precipitation. As shown in Figure 3.11, Si steel shows continuous enrichment of carbon in austenite, the Al steel has a similar behavior, but slightly drops in carbon concentration after 1000 s. Ref. steel and P steel both have a maximum in the carbon concentration curve, their curves showing a rapid increase at first, after 500 s, the carbon concentration decrease dramatically. That is due to the cementite precipitation, which consumes a large amount of carbon. The maximum comes from the competition between bainite transformation, which requires carbon to partition into austenite, and cementite precipitation, which consumes carbon

in the austenite. Al might be a potential element to replace Si in terms of retarding cementite precipitation; P has a small effects.

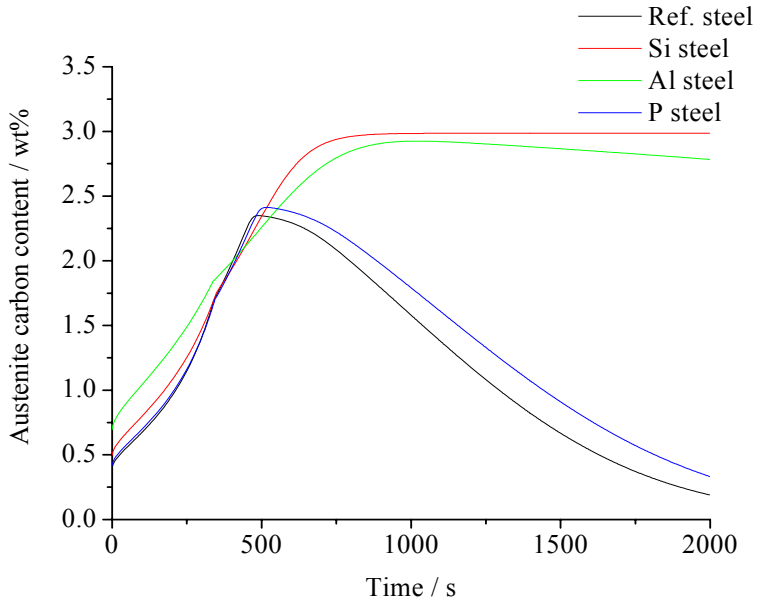

Figure 3.11: Carbon content of austenite as a function of bainitic holding time holding at 400℃ (intercritically annealed at 750 ℃).

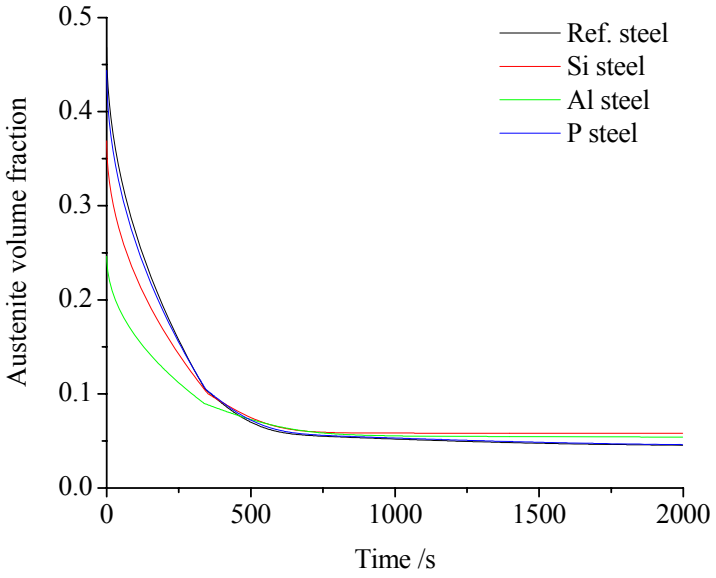

Figure 3.12: volume fraction of austenite as a function of bainitic holding time, holding at 400℃ (intercritically annealed at 750 ℃).

It can be seen in Figure 3.12 that the volume fraction of austenite decreases rapidly in the early stage, reacheing a steady state after 500 s for Si and Al steel, retained austenite is about 0.05. For Ref. steel and P steel, the volume fraction of austenite is still decreasing, given long enough time, it should go to zero.

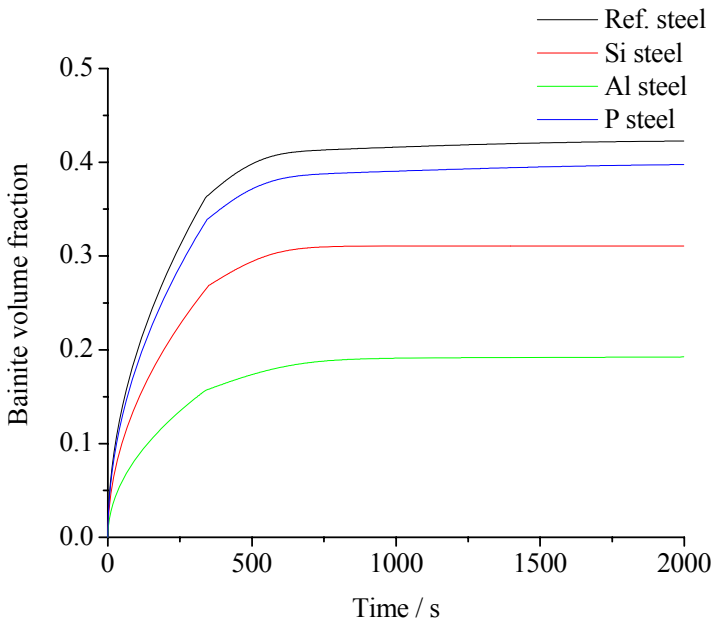

Figure 3.13: volume fraction of bainitic ferrite as a function of bainitic holding time, holding at 400℃ (intercritically annealed at 750 ℃).

While the volume fraction of austenite shows similar with each other for all the four steels, there is a big difference in the bainitic ferrite volume fraction shown in Figure 3.13. Due to the composition difference, after intercritical annealing, austenite volume fraction of the four steels is difference, therefore, leading to this result.

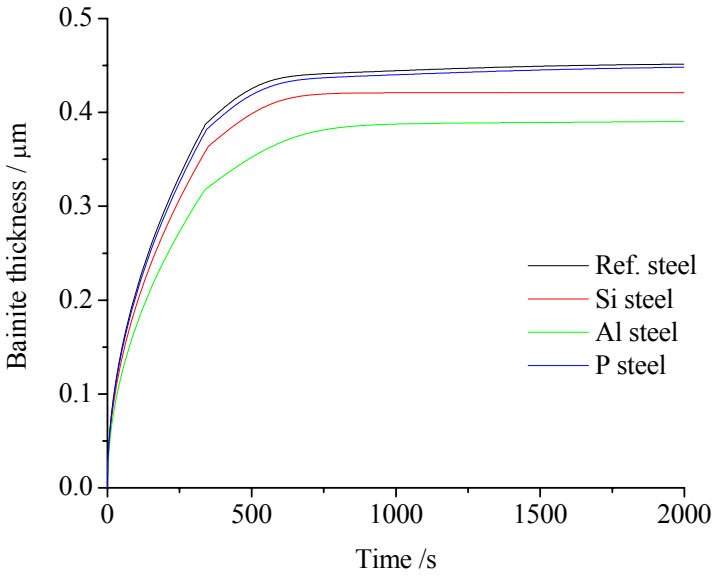

Figure 3.14: Thickening of bainitic ferrite as a function of bainitic holding time, holding at 400℃ (intercritically annealed at 750 ℃).

Solute elements also can affect the bainite growth rate. As the extrapolated paraequilibrium $\alpha / \alpha + \gamma$ boundary and Ae_3' line are similar shown in Figure 3.10, the driving force for all the steel transform into bainite at same temperature should be similar. As shown in Figure 3.14, Al steel grows slower than the others, so Al can slow down bainite transformation a lot, Si and P also have this effect, but smaller.

3.4.2 Influence of bainitic transformation temperature

The bainitic transformation temperature has a great influence on the kinetics of bainite reaction.

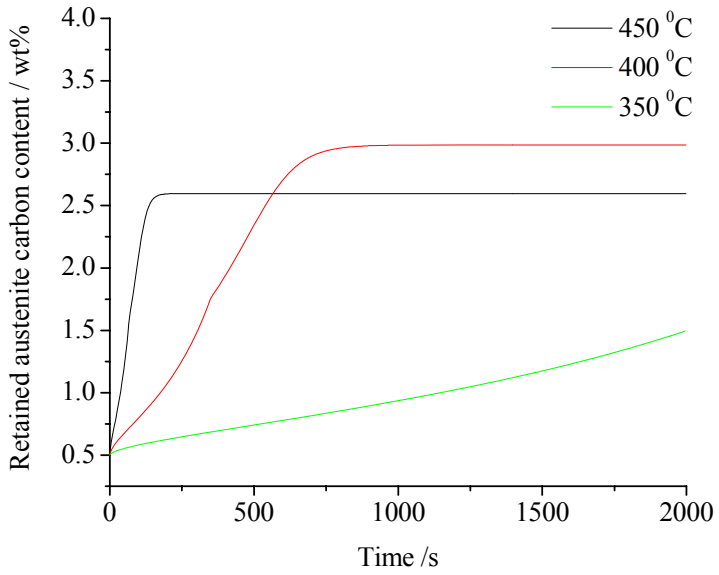

Figure 3.15: Carbon content of retained austenite as a function of bainitic holding time at 450, 400 or 350 ℃ (Si steel intercritically annealed at 750 ℃).

As for a diffusion controlled transformation, diffusivity is a key factor for the reaction rate. The diffusivity of carbon is strongly dependent on temperature, leading to a decrease of reaction rate as the temperature goes down. As shown in Figure 3.15, bainitic holding at 450 ℃ can finish reaction in very short time, but for 350 ℃, for 2000 s the reaction is still far from completion. Because Figure 3.15 shows the behavior of Si steel, it has no cementite precipitation, the carbon concentration of austenite increases continuously.

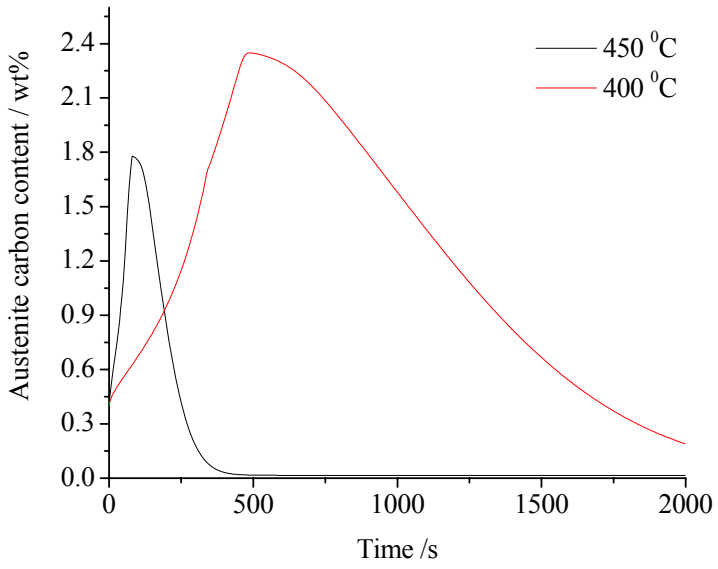

Figure 3.16: Carbon content of austenite as a function of bainitic holding time (Ref. steel intercritically annealed at 750℃).

Figure 3.16 shows the carbon content of austenite as a function of bainitic holding time for Ref. steel intercritically annealed at 750℃, for bainitic holding at 450 ℃. The carbon content of austenite reaches a maximum very rapidly, and then decreases rapidly, eventually reaches concentration where ferrite, austenite and cementite are in paraequilibrium (Si, P, Al and Cu are not forced to paraequilibrium, because of the lack of thermodynamic data). For holding at 400 ℃, maximum comes later, but higher than the former. As at higher temperatures, where the bainite reaction proceeds faster, carbon enrichment should be faster, but cementite precipitate faster as well, so at 450 ℃ the maximum value is lower than 400 ℃.

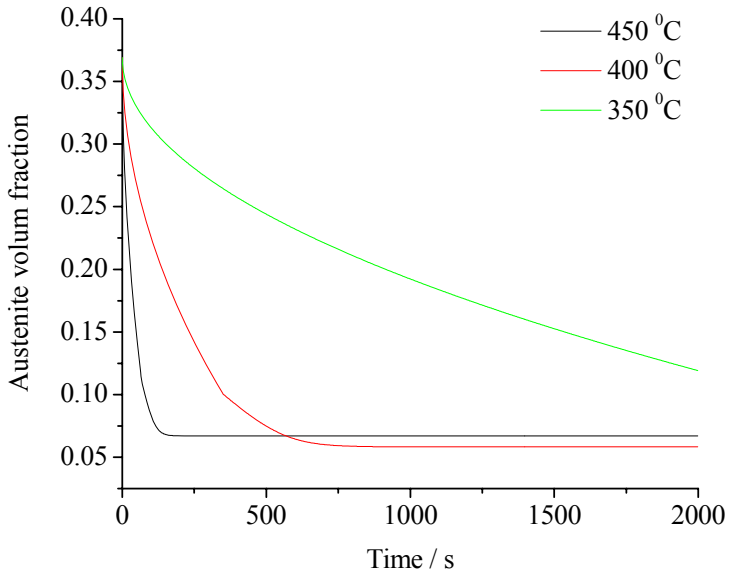

Figure 3.17: Volume fraction of austenite as a function of bainitic holding time at 450, 400 or 350 ℃ (Si steel intercritically annealed at 750 ℃).

As the bainitic holding temperature decreases, the austenite volume fraction should decrease shown in Figure 3.17. This is due to the model boundary condition, lower temperature leads to higher austenite carbon concentration in paraequilibrium with ferrite.

3.4.3 Influence of intercritical annealing temperature

Intercritical annealing affects the bainitic isothermal transformation by its influence on the initial austenite composition and volume fraction.

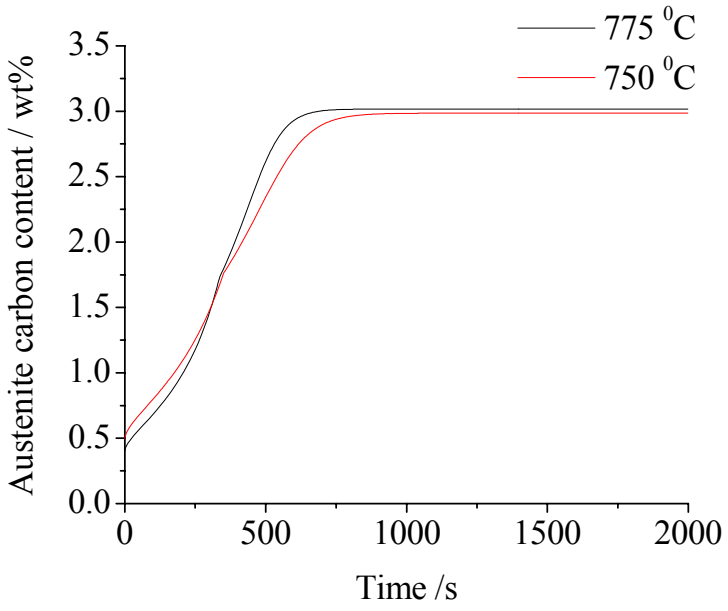

Figure 3.18: Carbon content of austenite as function of bainitic holding time at 400 ℃ (Si steel intercritically annealed at 775 or 750 ℃).

Figure 3.18 shows larger final carbon content than that of 750 ℃, also enrichment of carbon is faster, despite the initial carbon content is lower. Higher intercritical annealing leads to lower paraequilibrium carbon content in austenite which is clear in phase diagram, also higher temperature leads to faster carbon diffusion, which means a faster approach to paraequilibrium, so the starting carbon content of annealed at 775 ℃ should be lower than 750 ℃.

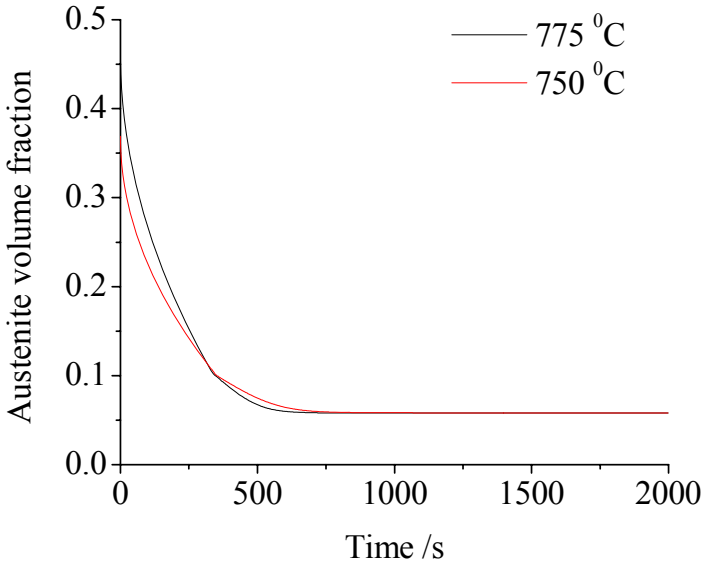

Figure 3.19: Austenite volume fraction as a function of bainitic holding time, holding at 400℃ (Si steel intercritically annealed at 775 or 750 ℃).

Retained austenite volume fraction is about 0.05 in this Si steel, which is a consequence of the paraequilibrium boundary condition for the diffusional model. This is not realistic as in high Si steel, reported retained austenite volume fraction in similar composition is usually about 0.1-0.2 [44, 61]

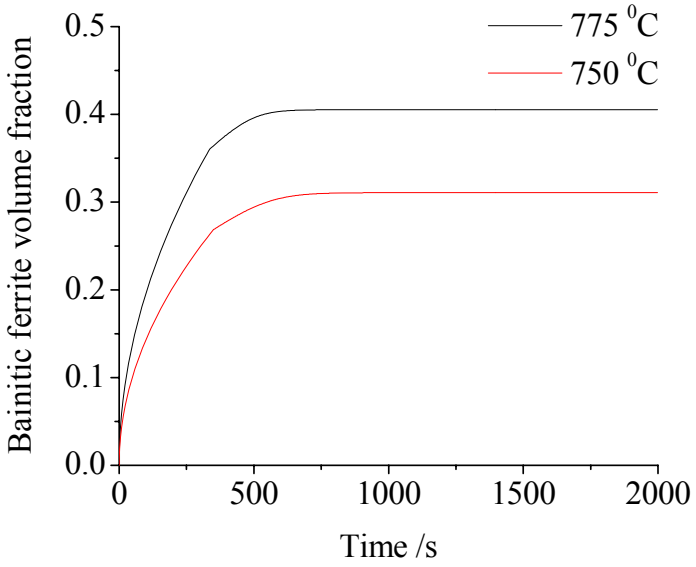

Figure 3.20: Bainitic ferrite volume fraction as a function of bainitic holding time, holding at 400℃ (Si steel intercritically annealed at 775 or 750 ℃).

Also higher intercritical annealing temperature leads to a larger austenite volume fraction shown in Figure 3.19, when it cooled to isothermal bainitic soaking temperature, the amount of austenite which can transform to bainitic ferrite is larger, shown in Figure 3.20, and this will lead to a higher growth rate of bainitic ferrite.

3.5 Summary

A theoretical framework for modelling the effect of Si addition on cementite nucleation kinetics has been developed.

-Si partition during cementite nucleation is impossible;

-Si addition retards the cementite nucleation rate by a factor of

$$R_J = \exp\{-(\Delta G^*/kT)[1/(1-x\Delta g_b/\Delta g_{\gamma/cm})^2 - 1]\}$$

Higher bainitic holding temperature leads to fast cementite precipitation in low Si steel.

Al can greatly slow down the carbon diffusion in bainite transformation, Si, P also have the same effect, but smaller.

Diffusional model is not good for the bainite transformation, as the reported carbon content in TRIP-assisted steel usually about 1-1.5 wt%, but the boundary condition for diffusional model is paraequilibrium carbon content, which is about 3 wt% in the temperature range of bainite isothermal transformation *i.e.* 350-450 ℃. Also diffusional model ignored the fact that there is a shear strain during bainite transformation. The model also does not distinguish between the atomic mechanism of bainite and allotriomorphic ferrite, so it is in principle possible to form bainite at the Ae_3 temperature in the scenario assumed.

IV Conclusions and Future Work

Multiphase TRIP-assisted steels are now an established class of low-alloy high-strength steels which have good uniform elongation and strength, due to the occurrence of the transformation induced plasticity phenomenon during deformation. The presence of austenite in the initial microstructure and its stability is critical to the achievement of the desired properties. The retention of austenite is usually achieved by the combined effect of an appropriate chemical composition and heat-treatment.

Paraquilibrium thermodynamic calculations show that the substitution of Si by P has little effect on Ae_1' and Ae_3' transformation temperatures. Replacement of Si by Al however shifts these temperatures to appreciably higher values and effectively eliminates the presence of a fully austenitic region.

Paraequilibrium will not be reached in typical intercritical annealing process times of around 3 minutes. The pearlite colony size has a big influence on the kinetics of austenitisation in intercritical annealing. Fine pearlite can accelerate austenite formation.

A theoretical framework for modelling the effect of Si addition on cementite nucleation kinetics has been developed. Si partition during cementite nucleation is assumed to be impossible; Si addition retards the cementite nucleation rate by a factor of:

$$R_J = \exp\{-(G^*/kT)[1/(1-x_{Si}\Delta g_b/\Delta g_{\gamma/cm})^2 - 1]\}$$

Higher bainitic holding temperature leads to fast cementite precipitation in low Si steel.

Al can greatly slow down the carbon diffusion in bainite transformation, Si, P also have the same effect, but smaller.

A more advanced transformation model will be necessary in order to fully understand the observed transformation behavior, especially the cementite precipitation model.

Future work

As demonstrated, the diffusional model of bainite transformation doesn't work well; due to the ignorance of the shear strain accompany the bainite transformation. The displacive mechanism will be necessary to be adopted in order to understand the bainite transformation behavior.

In handling the Si influence on cementite precipitation, back-calculation is used, the experimental data is most important to give a good result. Experimental verification has to be done, for there are not adequate data available in literatures. Also in cementite precipitation model, Avrami equation is used which is for constant growth rate that might be diverse from reality, so improvement is necessary.

V References

1. V.F. Zackay, E.R. Parker, D. Fahr, and R. Busch, *The Enhancement of Ductility in High-Strength Steel.* Transactions of the ASM, 1967. **60**: pp. 252-259.
2. O. Matsumura, Y. Sakuma, and H. Takechi, *Enhancement of elongation by retained austenite in intercritical annealed 0.4C-1.5Si-0.8Mn steel.* Transactions of the Iron and Steel Institute of Japan, 1987. **27**: pp. 570-579.
3. O. Matsumura, Y. Sakuma, and H. Takechi, *Trip and its kinetic aspects in austempered 0.4C-1.5Si-0.8Mn steel.* Scripta Metallurgica, 1987. **21**: pp. 1301-1306.
4. P.J. Jacques, *Transformation-induced plasticity for high strength formable steels.* Current Opinion in Solid State and Materials Science, 2004. **8**: p. 262.
5. ULSAB-AVC. [cited; Available from: http://www.worldautosteel.org/ulsab-avc/.
6. P.J. Jacques, E. Girault, and A. Mertens, *The Developments of Cold-rolled TRIP-assisted Multiphase Steels. Al-alloyed TRIP-assisted Multiphase Steels.* ISIJ International, 2001. **41**: pp. 1068-1074.
7. S. Jiao, F. Hassani, R.L. Donaberger, E. Essadiqi, and S. Yue, *The Effect of Processing History on a Cold Rolled and AnnealedMo–Nb Microalloyed TRIP Steel.* ISIJ International, 2002. **42**: pp. 299-303.
8. S.J. Kim, C.G. Lee, T.H. Lee, and C.S. Oh, *Effects of Copper Addition on Mechanical Properties of 0.15C-1.5Mn-1.5Si TRIP-aided Multiphase Cold-rolled Steel Sheets.* ISIJ International, 2002. **42**: pp. 1452-1456.

9. S. Hashimoto, S. Ikeda, K. Sugimoto, and S. MIYAKE, *Effects of Nb and Mo Addition to 0.2%C-1.5%Si-1.5%Mn Steel on Mechanical Properties of Hot Rolled TRIP-aided Steel Sheets.* ISIJ International, 2004. **44** pp. 1590-1598.

10. K. Sugimoto, N. Usui, M. Kobayashi, and S. Hashimoto, *Effects of Volume Fraction and Stability of Retained Austenite on Ductility of TRIP-aided Dual-phase Steels.* ISIJ International, 1992. **32**: pp. 1311-1318.

11. P.D. Hodgson, S. Yue, and A.Z. Hanzaki, *Hot Deformation Characteristics of Si-Mn TRIP Steels with and without Nb Microalloy Additions.* ISIJ International, 1995. **35**: pp. 324-331.

12. H.K.D.H. Bhadeshia, *Bainite in Steels*. second ed. 2001, London: IOM Communicatins Ltd. pp. 163-164.

13. G. Krauss, *Steels:Heat Treatment and Processing Principles*. ASM International. 1989, OH, USA. pp. 52-53.

14. A.I. Katsamas, G.N. Haidemenopoulos, and A.N. Vasilakos, *Simulation of intercritical annealing in low-alloy TRIP steels.* steel research, 2000. **71**: pp. 351-356.

15. C. Scott and J. Drillet. *Quantitative analysis of local carbon concentrations in TRIP steels*. in *Proc. Intern. Conf. on TRIP-aid High Strength Ferrous Alloys*. 2002. Ghent, Belgium.

16. H.K.D.H. Bhadeshia, *The Bainite transformation: Unresolved issues.* Materials Science and Engineering A, 1999. **273-275**: pp. 58-66.

17. P.J. Jacques, F. Delannay, X. Cornet, P. Harlet, and J. Ladriere, *Enhancement of the mechanical properties of a low-carbon, low-silicon steel by formation of a multiphased microstructure containing retained Austenite.* Metallurgical and

Materials Transactions A, 1998. **29**: pp. 2383-2393.

18. W. Bleck. *Using the TRIP Effect - The Dawn of a Promising New Group of Cold Formable Sheets,*. in *International Conference on TRIP-Aided High Strength Ferrous Alloys*. 2002. Ghent: GRIPS.

19. J. Mahieu, B.C.D. Cooman, J. Maki, and S. Claessens, *Hot-Dip Galvanizing of Al Alloyed TRIP Steels.* Iron & Steelmaker, 2002. **29**: pp. 29-34.

20. I. Tsukatani, S. Hashimoto, and T. Inoue, *Effects of Silicon and Manganese Addition on Mechanical Properties of High-strength Hot-rolled Sheet Steel Containing Retained Austenite.* ISIJ International, 1991. **31**: pp. 992-1000.

21. H.C. Chen, H. Era, and M. Shimizu, *Effect of Phosphorus on the Formation of Retained Austenite and Mechanical Properties in Si-Containing Low-Carbon Steel Sheet.* Metallurgical and Materials Transactions A, 1989. **20**: pp. 437-445.

22. B.C. De Cooman, *Structure-properties relationship in TRIP steels containing carbide-free bainite.* Current Opinion in Solid State and Materials Science, 2004. **8**(3-4): pp. 285-303.

23. B. Mintz, *Hot Dip Galvanizing of Transformation Induced Plasticity and Other Intercritically Annealed Steels.* International Materials Reviews, 2001. **46**: pp. 169-197.

24. M.D. Meyer, D. Vandershueren, and B.C.D. Cooman, *The Influence of the Substitution of Si by Al on the Properties of Cold Rolled C-Mn-Si TRIP Steels.* ISIJ International, 1999. **39**: pp. 813-822.

25. W.C. Leslie and G.C. Rauch, *Precipitation of Carbides in Low-Carbon Fe-Al-C Alloys.* Metallurgical and Materials Transactions A, 1978. **9**: pp. 343-349.

26. J. Mahieu, D.V. Dooren, L. Barbe, and B.C.D. Cooman. *Influence of Al, Si and P*

on the kinetics of intercritical annealing of TRIP-aided steels: thermodynamical prediction and experimental verification. in *International Conference on TRIP-Aided High Strength Ferrous Alloys* 2002. Ghent: GRIPS.

27. A.Z. Hanzaki, P.D. Hodgson, and S. Yue, *The Influence of Bainite on Retained Austenite Characteristics in Si-Mn TRIP Steels.* ISIJ International, 1995. **35**: pp. 79-85.

28. A.Z. Hanzaki, P.D. Hodgson, and S. Yue, *Retained Austenite Characteristics in Thermomechanically Processed Si-Mn Transformation-Induced Plasticity Steels.* Metallurgical and Materials Transactions A, 1997. **28**: pp. 2405-2414.

29. A. Lucas, J.C. Herman, and A. Schmitz. *Cu-Containing TRIP steels*. in *International Conference on TRIPAided High Strength Ferrous Alloys*. 2002. Ghent: GRIPS.

30. S. Traint, A. Pichler, K. Hauzenberger, P. Stianszy, and E. Werner. *Influence of Silicon, Phosphorus, and Copper on the Phase Transformations of Low Alloyed TRIP-steels*. in *International Conference on TRIP-Aided High Strength Ferrous Alloys*. 2002. Ghent: GRIPS.

31. A. Pardo, M.C. Merino, M. Carboneras, F. Viejo, R. Arrabal, and J. Munoz, *Influence of Cu and Sn content in the corrosion of AISI 304 and 316 stainless steels in H2SO4.* Corrosion Science, 2006. **48**(5): pp. 1075-1092.

32. A.I. Katsamas, G.N. Haidemenopoulos, and N. Aravas, *Modelling of Transformation in TRIP Steels.* steel research international, 2004. **75** pp. 737-743.

33. H.K.D.H. Bhadeshia, *Bainite in Steels*. second ed. 2001, London: IOM Communicatins Ltd. pp. 232-233.

34. C. Zener, *Theory of Growth of Spherical Precipitates from Solid Solution.* Journal

of Applied Physics, 1949. **20**: pp. 950-953.

35. J.W. Christian, *The Theory of Transformations in Metals and Alloys*. third ed. 2002, Oxford: Pergamon. pp. 491.

36. J.D. Robson and H.K.D.H. Bhadeshia, *Modelling precipitation sequences in power plant steels Part 1 - Kinetic theory.* Materials Science and Technology, 1997. **13**: pp. 631-639.

37. Z. Li and D. Wu, *Study of the high strength and low yield ratio cold forging steel.* Materials Science and Engineering A 2007. **452**: p. 144.

38. P.R. Howell, *The Pearlite Reaction in Steels: Mechanisms and Crystallography.* Materials Characterization, 1998. **40**: pp. 231-232.

39. A.M. Elwazri, P. Wanjara, and S. Yue, *The effect of microstructural characteristics of pearlite on the mechanical properties of hypereutectoid steel.* Materials Science and Engineering A, 2005. **404**: p. 93.

40. H.K.D.H. Bhadeshia. *MAP_STEEL_DIFFUS*. [cited; Available from: http://www.msm.cam.ac.uk/map/steel/subs/diffus-b.html.

41. H.K.D.H. Bhadeshia, *Diffusion of carbon in austenite.* Metal Science, 1981. **15**: pp. 477-479.

42. S.S. Babu and H.K.D.H. Bhadeshia, *Diffusion of carbon in substitutionally alloyed austenite.* Journal of Materials Science Letters, 1995. **14**: pp. 314-316.

43. E. Girault, A. Mertens, P. Jacques, Y. Houbaert, and B. Verlinden, *Comparison of the effects of silicon and aluminium on the tensile behaviour of multiphase TRIP-assisted steels.* Scripta Materialia, 2001. **44**: pp. 885-892.

44. P.J. Jacques, E. Girault, P. Harlet, and F. Delannay, *The Developments of Cold-rolled TRIP-assisted Multiphase Steels. Low Silicon TRIP-assisted*

Multiphase Steels. ISIJ International, 2001. **41**: pp. 1061-1067.

45. X.J. Jin, N. Min, K.Y. Zheng, and T.Y. Hsu, *The Effect of Austenite Deformation on Bainite Formation in an alloyed eutectoid steel.* Materials Science and Engineering A, 2006. **438–440**: pp. 170–172.

46. W.Z. Chen, T.Y. Hsu, S.C. Chen, and J.H. Zhang, *The internal friction of the pearlitic, bainitic and martensitic transformations in Fe-Ni-C alloys.* Acta Metallurgica et Materialia, 1990. **38**: pp. 2337-2342.

47. T.Y. Hsu and Y.W. Mou, *Thermodynamics of the bainitic transformation in Fe-C alloys.* Acta Metallurgica, 1984. **32**: pp. 1469-1481.

48. H.K.D.H. Bhadeshia and D.V. Edmond, *The mechanism of bainite formation in steels.* Acta Materialia, 1980. **28**: pp. 1265-1273.

49. M. Takahashi, *Recent progress: kinetics of the bainite transformation in steels.* Current Opinion in Solid State and Materials Science, 2004. **8**: pp. 213-217.

50. H.K.D.H. Bhadeshia. [cited; Available from: http://cml.postech.ac.kr/a/lecture6.pdf.

51. H.S. Fang, J.B. Yang, Z.G. Yang, and B.Z. Bai, *The mechanism of bainite transformation in steels.* Scripta Materialia, 2002. **47**: pp. 157-162.

52. A.K. Srivastava, G. Jha, N. Gope, and S.B. Singh, *Effect of heat treatment on microstructure and mechanical properties of cold rolled C-Mn-Si TRIP-aided steel.* Materials Characterization, 2006. **57**: pp. 127-135.

53. T.D. Cock, J.P. Ferrer, C. Capdevila, F.G. Caballero, V. Lopez, and C.G.d. Andres, *Austenite retention in low Ai/Si multiphase steels.* Scripta Materialia, 2006. **55**: pp. 441-443.

54. C.P. Scott and J. Drillet, *A study of the carbon distribution in retained austenite.*

Scripta Materialia, 2007. **56**: pp. 489-492.

55. H.K.D.H. Bhadeshia, *Bainite in Steels*. second ed. 2001, London: IOM Communicatins Ltd. pp. 63.

56. K. Avrami, *Kinetics of Phase Change 1.* Journal of Chemical Physics, 1939. **7**: pp. 1103-1112.

57. K. Avrami, *Kinetics of Phase Change 2.* Journal of Chemical Physics, 1940. **8**: pp. 212-224.

58. K. Avrami, *Kinetics of Phase Change 3.* Journal of Chemical Physics, 1941. **9**: pp. 177-184.

59. K. Sugimoto, M. Tsunezawa, T. Hojo, and S. Ikeda, *Ductility of 0.1–0.6C–1.5Si–1.5Mn Ultra High-strength TRIP-aided Sheet Steels with Bainitic Ferrite Matrix.* ISIJ International, 2004. **44**: pp. 1610.

60. K. Sugimoto, T. Iida, J. Sakaguchi, and T. Kashima, *Retained Austenite Characteristics and Tensile Properties in a TRIP Type Bainitic Sheet Steel.* ISIJ International, 2000. **40**: pp. 903-904.

61. P. Jacques, E. Girault, T. Catlin, N. Geerlofs, T. Kop, S.v.d. Zwaag, and F. Delannay, *Bainite tranaformation of low carbon Mn-Si TRIP-assisted multiphase steels: influence of Si content on cementie precipitaion and austenite retention.* Materials Science and Engineering, 1999. **A 273-275**: pp. 475-479.

Acknowledgements

I am indebted Professor Weijie Liu and Professor H.K.D.H. Bhadeshia for their supervision, encouragement and enthusiasm during the work. Thanks to Professor Rongshan Qin for giving me so much advice and Professor In Gee Kim for organizing our group so nicely.

Dr Steve Ooi deserves great thanks for his help on this work, and Mr Qin Bo for spent so much time together discussing about problems in research and course work. Thanks all the members especially the Koreans in CML for helping me so much during my stay, making my life a really enjoyable one. Thanks Mr Young Bhum Kim for helping with the computer problems.

I would like to thank Graduate Institute of Ferrous Technology and POSCO for their financial support.

Finally, I would like to record my deep sense of appreciation for my parents and sister for everlasting support for me, in spite of all their hardship.

CURRICULUM VITAE

Name: Guo, Lei (郭磊)

Date of birth：26 September 1982

Place of birth: Hunan province, P. R. China

Address: Jin Ke Yuan Xiao Qu, Lao dong dong lu,
Changsha, P. R. China. 410000

Education:

M. S. 2007, POSTECH (Pohang, Korea), Graduate Institute of Ferrous Technology, Computational Metallurgy.

B. S. 2005 Chongqing University (Chongqing, P. R. China), Metallurgy Engineering.